In_xSe_y ALLOY THIN FILMS FOR PHASE CHANGE RANDOM ACCESS MEMORY (PRAM) APPLICATIONS

WEKUNDA B. Z. BUYA (B. Ed. Sci)
I56/13090/2005

A thesis submitted in partial fulfillment of the requirements for the award of the degree of Master of Science (Electronics and Instrumentation) in the School of Pure and Applied Sciences of Kenyatta University

July 2013

DECLARATION

This thesis is my original work and has not been presented for the award of a degree or any other award in any University.

WEKUNDA B. Z. BUYA	Signature	Date
Department of Physics	……………….	………………

Kenyatta University

P.O BOX 43844-00100

NAIROBI-KENYA

This thesis has been submitted for examination by our approval as university supervisors.

DR PATRICK M. KARIMI	Signature	Date
Department of Physics	…………….	……………

Kenyatta University

P.O BOX 43844-00100

NAIROBI-KENYA

DR. WALTER K. NJOROGE	Signature	Date
Department of Physics	……………….	………………

Kenyatta University

P.O BOX 43844-00100

NAIROBI-KENYA

DEDICATION

This thesis is dedicated to my lovely wife Sophie, my daughters; Gift and Delight and my son Davy.

ACKNOWLEDGEMENTS

It is with great pleasure that I recognize the input of a number of special people without whom this project could have stalled. Firstly, I honor God the Almighty for the gift of life and providence to see this work through. Secondly, to my supervisors Dr. Patrick M. Karimi and Dr. Walter K. Njoroge of Kenyatta university to whom I am greatly indebted. I register my appreciation to them especially for their insight and wisdom in the subject matter. Their input in this project is matchless. May the Almighty God bless them indeed.

Thirdly, I wish to pay tribute to the entire Master of Science class of 2006 among them; Erick Jobunga, James Mugambi, John Agumba, Nickson Zavani, Jeremiah Kebwaro, Livingstone Ochilo, and Enock Okiambe. John Agumba deserves special mention for assembling the Four Point Probe system and the accompanying software used during electrical characterization of the samples. I wouldn't forget to mention Abraham Tuwei and Enock Omayio for the partnership while pursuing this dream. Their input was invaluable. Special thank you to Simon Njuguna, the chief technician and the entire technical staff of Kenyatta University's physics department. Cornelius Waswa of Kenyatta University's Chemistry department is worth of mention for his input during sample fabrication.

I am grateful to my lovely wife Sophie for her prayers, encouragement, and patience throughout this period. Last but not least, the National Council for Science and Technology (NACOST) for awarding me a grant under the Science and Technology for Innovation (STI) program.

TABLE OF CONTENTS

DECLARATION ii

DEDICATION iii

ACKNOWLEDGEMENTS iv

TABLE OF CONTENTS v

LIST OF TABLES x

LIST OF FIGURES xi

ABBREVIATIONS, SYMBOLS AND ACRONYMNS xiii

ABSTRACT xv

CHAPTER ONE 1

INTRODUCTION 1

1.1 Background to the Study 1

1.2 Statement of the Research Problem 3

1.3 Objectives 4

1.3.1 Main Objective 4

1.3.2 Specific Objectives 4

1.4 Rationale 4

CHAPTER 2 8

LITERATURE REVIEW **8**

2.1 Introduction 8

2.2 Related studies 11

CHAPTER THREE **15**

THEORETICAL BACKGROUND **15**

3.1 Introduction 15

3.2 Volatile memory 15

3.3 Non-Volatile memory 15

3.3.1 Read Only Memory 16

3.3.2 Erasable Programmable Read Only Memory 16

3.3.3 Electrically Erasable Programmable Read Only Memory 17

3.3.4 Silicon Oxide Nitride Oxide Semiconductor 19

3.3.5 Ferroelectric Random Access Memory 20

3.3.6 Magnetic Random Access Memory 21

3.3.7 Nanocrystal Memory 22

3.3.8 Phase Change Random Access Memory 22

3.4 Thin film Deposition 25

3.4.1 Theory of crystallization 26

3.4.1.1 Nucleation and crystal growth in chalcogenide glasses 26

3.4.1.2 Thermal analysis 29

3.4.2. Chemical Vapor Deposition 32

3.4.2.1. Liquid Vapor Epitaxy 32

3.4.2.2. Vapor Phase Epitaxy..33

3.4.2.3. Molecular Beam Epitaxy 34

3.4.3. Physical Vapor Deposition 35

3.4.3.1 Sputtering..35

3.4.3.2 Evaporation..36

3.5 Optical characterization 39

3.5.1 Optical Reflectance 39

3.5.2 Optical transmission..39

3.5.3 Absorption of light 40

3.5.4 Dielectric function..41

3.5.5 Refractive Index 43

3.5.6 Optical penetration depth 44

3.5.7 Determination of band gap 44

3.6 Electrical Characterization 46

3.6.1 Electrical resistivity of Semiconductors 46

3.6.2 Sheet Resistivity of thin films 48

3.7 Theory of Device 0peration..49

CHAPTER FOUR..51

MATERIALS AND METHODS 51

4.1 Introduction 51

4.2 Synthesis of Indium and Selenium..51

4.3 In_xSe_y Thin Film Preparation 52

4.4 Thin Film Thickness Measurement. 52

4.5 Optical Characterization of the Films. 53

4.5.1 Optical band gap of the films 54

4.6 Electrical Characterization. 56

4.6.1 The Four Point Probe Technique 56

4.7 Device Fabrication 57

4.7.1 Aluminum Anode back contact layer 58

4.7.2. $InSe_3$ Thin Film layer....................59

4.7.3 Silver Cathode top electrode 59

4.8 PRAM test device testing 60

CHAPTER FIVE....................61

RESULTS AND DISCUSSION 61

5.1 Introduction 61

5.2 Optical Characterization of the films 61

5.2.1 Optical properties 61

5.2.1.1 Transmittance, Reflectance and Absorbance 61

5.2.1.2 Energy band gaps of In_xSe_y films....................64

5.2.1.3 Refractive index of the film samples 67

5.3 Electrical properties of the thin films....................68

CHAPTER SIX....................74

CONCLUSION AND RECOMMENDATIONS **74**

6.1 Conclusion 74

6.2 Recommendations 75

REFERENCES **77**

APPENDICES **83**

Appendix 1: Edwards AUTO 306 Vacuum coater 83

Appendix 2: Photograph of Alpha IQ Surface Profiler 84

Appendix 3: Photograph of the set used during thermal annealing 85

LIST OF TABLES

Table 3.1: A summary of the various memory technologies and their attributes 25

Table 5.1: Summary of the band gap energies of the films under investigation..............66

Table5.2: Indium/ Selenium ratio and the sheet resistivity at room temperature..............68

Table 5.3: Summary of the variation of the crystallization temperature with Indium/Selenium ratio. 72

LIST OF FIGURES

Figure 3.1: Schematic diagram of a floating gate device 16

Figure 3.2: A schematic diagram of the cross-sectional view of PRAM cell structure....24

Figure 3.3: DC magnetron sputtering process utilizes dc gaseous exchange (Ohring,.....35

Figure 3.4: Schematic diagram of vacuum evaporation process for metallization 37

Figure 3.5: Schematic representation of the Interaction of light with the thin film..........40

Figure 3.4: Graphical determination of band gap energies Adapted from Palik, E.D. 45

Figure 4.1: Schematic diagram showing optical transmission measurements. 54

Figure 4.2: Plot of the square of absorption coefficient (α^2) against photon energy 55

Figure 4.3: Schematic diagram of four-point probe resistivity measurement using the Van der Pauw method..56

Figure 4.4: Schematic representation of set up used during sheet resistivity measurements at different temperatures. 57

Figure 4.5: Schematic diagram of vertical cross- section of PRAM test device 58

Figure 4.6: Masking of one side of slide before the layer of In_xSe_y is added. 59

Figure 4.7: Schematic illustration of the aerial view of the Phase Change Memory test device 60

Figure 5.1: Spectral graph of percentage reflectance against wavelength for thin films of Indium and Selenium in various ratios 62

Figure 5.2: Spectral graph of percentage transmittance against wavelength for films of indium and selenium in various ratios 63

Figure 5.3: A graph of sample fitting of experimental and simulated data....................64

Figure 5.4: Graphical determination of band gap of InSe thin film 65

Figure 5.5: Graphical variation of band gap energy with Indium to Selenium concentration in the films. 66

Figure 5.6: Spectral Graphs of refractive index against photon energy for the as deposited film samples of Indium and Selenium. 67

Figure 5.7: Graphical variation of Sheet resistivity with Indium to Selenium concentration in the film samples....69

Figure 5.8: Graphical variation of sheet resistivity against temperature during thermal cycling....70

Figure 5.9: Derivative of sheet resistivity against temperature for InSe film 71

Figure 5.10: Static mode I-V characteristics of $InSe_3$ PRAM test device. 73

ABBREVIATIONS, SYMBOLS AND ACRONYMNS

£	Pound
CD-RW	Compact disk rewritable
CMOS	Complementary metal oxide semiconductor
CVD	Chemical vapor deposition
DRAM	Dynamic random access memory
DVD-RW	Digital versatile drive rewritable
EEPROM	Electrically erasable programmable read only memory
E_g	Optical energy band gap
EOT	Equivalent oxide thickness
EPROM	Electrically programmable read only memory
FeRAM	Ferroelectric random access memory
FLOTOX	Floating gate tunneling oxide
FN	Fowler Nodheim
GMR	Giant magnetoresistive
GST	Germanium, antimony and Telluride
HEI	Hot electron injection
ITRS	International technology roadmap for semiconductors
k	Extinction coefficient
LVE	Liquid vapor epitaxy
MBE	Molecular beam epitaxy
MOCVD	Metal oxide chemical vapor deposition
MOSFET	Metal oxide semiconductor field effect transistor

MRAM	Magnetic random access memory
n	Refractive index
NC	Nanocrystal
OMVPE	Organometallic vapor phase epitaxy
PC	Phase change
PRAM	Phase change random access memory
PVD	Physical vapor deposition
PZT	Lead zirconate titanate
RF	Radio frequency
RTCVD	Rapid thermal chemical vapor deposition
SOC	Systems on chip
SONOS	Silicon oxide nitride oxide semiconductor
SRAM	Static random access memory
TMR	Tunneling magnetoresistive effect
TTRAM	Twin transistor random access memory
VPE	Vapor phase epitaxy
Z-RAM	Zero capacitor random access memory
α	Alpha
ε	Epsilon
π	Pi
ρ_s	Sheet resistivity
σ	Conductivity
Γ	Mass evaporation rate

ABSTRACT

Indium Selenide (In_xSe_y) has shown great advantages over the conventionally used $Ge_2Sb_2Te_5$ as a phase change memory material (PCM). It has been established that the electrical resistivity of Indium-Selenide based memory cell can be varied by a factor of 10^5 related with the degree of crystallization as compared with 10^3 for $Ge_2Sb_2Te_5$. It is this wider change of electrical resistivity and higher electrical resistivity that has attracted great attention to Indium-Selenide based phase change material. However, little if any, has been reported about the concentration of indium and selenium in the film and its effect on the resistivity of the In_xSe_y phase change alloy. In this study, the relationship between indium and selenium concentration, and electrical resistivity of thin films has been investigated. Also, the optical properties like the reflectance, transmittance, energy band gaps of the films have been studied. The films were fabricated by vacuum evaporation after synthesizing Indium and Selenium in various ratios by mass. Synthesis was done by melting them together in silica tube above 600 ^{0}C then left to cool before evaporating them on glass substrates in a high vacuum chamber maintained at ultra low pressure. The resistivity measurements were performed using the four point probe technique where the voltage and current were sourced from a sourcemeter interfaced to a labVIEW running computer. The film thickness measurements were carried out using Alpha IQ Surface Profiler and ranged from 80 nm to 120 nm. Films with a high concentration of indium were more reflective beyond the visible region while those with high concentration of selenium show more transmission beyond the visible region. The film with the highest concentration of selenium had a high energy band gap at 2.67 eV whereas that with the highest concentration of indium had the lowest band gap at 2.07 eV. The films with the highest concentration of indium exhibited greater resistance with sheet resistivity of about 109.6 Ωcm at room temperature and had the highest crystallization temperature of 203.3 ^{0}C. The fabricated PRAM device had static mode on voltage at 0.9 V and an off voltage of -0.4 V.

CHAPTER ONE

INTRODUCTION

1.1 Background of the Study

Phase change memory otherwise called phase change random access memory (PCM) is one of the promising non-volatile memories for the next generation portable electronics. Compared to Flash memory which is the most commonly used non- volatile memory PRAM has fast switching speed, low programmable energy, large sensing margin and excellent scalability. Furthermore, the switching current and device reliability can be improved by further reducing the design rule. A multibit per cell operation is also possible. Thus, very extensive research and development work is currently being conducted in order to commercialize PRAM either as a standalone memory or as a memory unit for systems on chip (SOCs) (Pellizer *et al.,* 2004).

Since PRAM makes use of the reversible phase transition of chalcogenide-based materials, the data is stored as crystalline states of the chalcogenide resistor. The basic switching mechanism of PRAM can be explained in terms of phase transition between its amorphous and crystalline states as follows. The crystalline state of the chalcogenide material is controlled by means of an electric pulse (Lai *et al.,* 2001). Using a high voltage and a short duration pulse, the phase change resistor is heated up to its melting temperature and then quenched. In this way the phase of the chalcogenide becomes amorphous and develops high electrical resistance. The phase change (PC) resistor with an amorphized region is then returned to the crystalline phase using a low voltage and

relatively long duration pulse. Due to the low voltage pulse, the temperature of the phase change resistor is increased, but cannot reach to the melting temperature. When the phase change resistor with an amorphized region is heated, nucleation and growth of crystalline phase occurs and the amorphous region becomes crystalline. Consequently, the electrical resistance of resistor is also returned. The switching requires relatively large current to heat up the phase change resistor and to create thermally induced transition. Since the electric resistivity of the amorphous chalcogenide is orders of magnitude higher than that of crystalline chalcogenide, phase transition of chalcogenide transistor can easily be sensed by applying the low bias voltage. The dramatic differences in the electric resistivity of amorphous and crystalline states of chalcogenide based materials forms the basis by which data are stored. The amorphous high resistance state is used to represent a binary 0, and the crystalline, low resistance state represents a 1.

Most studies of PRAM are based on the germanium, antimony, and tellurium ($Ge_2Sb_2Te_5$) called GST, compound, (Lai *et al.,* 2001; Pellizer *et al.,* 2004), which is a mixture of GeTe and Sb_2Te_3. The compound was originally developed for use in the recording media of optical data storage devices, such as CD-RW and DVD-RW. In those instances, the material's optical properties are manipulated rather than its resistivity, as chalcogenide refractive index has been found to change with the state of the material. Like other chalcogenide phase change material, $Ge_2Sb_2Te_5$ shows a reversible phase transition between amorphous and crystalline phases. The as-sputtered, amorphous $Ge_2Sb_2Te_5$ compound can be crystallized by isothermal annealing and can also be amorphized by rapid heating above its melting temperature followed by

quenching. This way, the electrical resistivity of $Ge_2Sb_2Te_5$ is varied by up to 10^3 times by amorphization.

Indium based chalcogenide has several advantages over GST which has widely been used for phase change resistor. Among the advantages are:-

(i) The electric resistivity of In_2Se_3 can be varied by the factor of 10^5 with crystallization where crystalline-phase In_xSe_y has much higher resistivity than crystalline $Ge_2Sb_2Te_5$ Thus the switching power can be delivered more effectively due to its higher resistivity.

(ii) Since In_2Se_3 is thermodynamically stable (Vassiliev *et al.,* 1998) and is single-phase binary compound, low melting temperature compound is not formed, and thus phase decomposition-related device failure can be avoided.

(iii) Since In-Se amorphous network structure is weak, faster crystallization can be achieved.

1.2 Statement of the Research Problem

Research on phase change memory cell, has been based on $Ge_2Sb_2Te_5$ as the compound of interest until recently when In_2Se_3 proved more advantageous. Though several researches have been conducted to assert the place of In_2Se_3 thin film as the best material for phase change memory, the quality and properties of a given thin film depends on growth conditions and techniques (Ohring, 1992). Various techniques have so far been employed which include co-evaporation of elemental In and Se at room temperature

(Heon, 2005). However not much has been mentioned about the relationship between film resistivity and the ratio of In-Se composition. In this study, we investigate the relationship between the In-Se concentration and the sheet resistivity.

1.3 Objectives

1.3.1 General Objective

The main objective in this work was to investigate the relationship between the In-Se concentration and the sheet resistivity at room temperature and during annealing.

1.3.2 Specific Objectives

The specific objectives were:-

(i) To synthesize In_xSe_y in various compositions by mass and prepare thin films of the samples on glass substrates by single source evaporation.

(ii) To determine the sheet resistivity of the various thin films at room temperature and during annealing.

(iii) To perform optical spectroscopy on the various In_xSe_y compositions to determine the bandgap energy, E_g, and other optical constants which include; the refractive index, n, the film thickness t, the dielectric function ε, absorption coefficient α, and the extinction coefficient k.

(iv) To fabricate a PRAM and determine I-V characteristics.

1.4 Rationale

As many newly developed digital electronic devices, such as digital cameras, and camcorders, MP3 players and smart phones, among others become popular, the demand

for non-volatile semiconductor memory is increasing. Currently Flash memory (NAND type) with a number of practical problems like scaling difficulties as chip lithography shrinks is the only available non-volatile memory and, thus, its market is expanding rapidly. Phase change random memory (PRAM) is a new non-volatile memory which uses reversible phase transition of chalcogenide resistor. It has several advantages including: extremely large read dynamics range, reduced switching current, improved device size and a potential multibit per cell operation. Hence, intensive research is underway to commercialize PRAM both as a standalone non-volatile memory and as a memory unit for system on a chip (Ovshinsky, 1968; Hwang *et al,. 2003).*

To date however, much of the research has centered on the use of a chalcogenide alloy of germanium, antimony and tellurium (GST). Although it has not yet reached commercialization stage for consumer electronic devices, nearly all prototype devices make use of GST. The phase transition process in this alloy can be completed in as quickly as five nanoseconds, according to a January 2006 Samsung patent application concerning this technology. This is comparable to conventional volatile memory device, for instance, modern DRAM cells have a switching time on the order of two nanoseconds.

A more recent advance pioneered by Intel and STMicroelectronics allows the materials state to be more carefully controlled, allowing it to be transformed into one of four states, two of which are partially crystalline. Each of these states has different electrical properties that can be measured during reads, allowing a single cell to represent two bits,

doubling memory density (Green, 2008). Many factors influence the suitability of a memory structure for a particular application, however, it is the switching time that makes PRAM, and other replacements of Flash memory most interesting. PRAM offers much higher performance in applications where writing quickly is important, both because the memory elements can be switched more quickly, and also because single bits may be changed to either 1 or 0 without needing to first erase an entire block of cells. PRAM's high speed, thousands of times quicker than conventional hard devices make it particularly interesting in non-volatile memory roles that are currently performance limited by memory access speed.

Compared to flash devices, PRAM devices degrade slowly. A PRAM device may endure around 100 million write cycles (Intel, 2008). PRAM lifetime is limited by mechanisms such as degradation due to GST thermal expansion during programming, metal (and other material) migration, and other mechanisms still unknown. Whereas flash devices trap electrons to store information; they are susceptible to corruption from radiation, making them unsuitable for many space and military applications. However, PRAM exhibits higher resistance to radiation and therefore a preferable replacement.

The special gates in Flash memory "leak" charge (electrons) with time causing corruption and loss of data. The resistivity of the memory element in PCM is more stable, allowing data retention for years or decades, even at elevated temperatures (Intel 2008). It is against this backdrop that PRAM of Indium Selenide based memories have attracted great attention in research. This study was meant to investigate the relationship between

the concentration of indium and selenium in the film, and its effect on the sheet resistivity of the films which has an influence on the switching behavior of PRAM.

CHAPTER 2

LITERATURE REVIEW

2.1 Introduction

As highlighted in chapter one, much research is currently being undertaken in order to commercialize PRAM as an alternative to Flash memory due to the latter's limitations mentioned earlier. Previous work on PRAM however, focused more on chalcogenide GST material which recent work shows suffers limitations compared to the alloy of indium and selenium as mentioned in chapter one. Currently focus is more on Indium Selenide which has an upper hand in comparison with GST alloy.

The greatest challenge for phase change memory has been the requirement of high programming current density ($\geq 10^7 Acm^{-2}$) in the active volume. This has led to the active areas which are much smaller than the driving transistor area. The discrepancy has forced phase change memory structures to package the heater and sometimes the phase change material itself in sublithographic dimensions. This is a process cost disadvantage compared to Flash. The contact between the hot phase change region and the adjacent dielectric is another fundamental concern. The dielectric may begin to leak current at higher temperature, or may lose adhesion when expanding at a different rate from the phase change material.

Phase change memory is susceptible to a fundamental trade-off of unintended against intended phase change. This stems directly from the fact that the phase change is a

thermally driven process rather than an electronic process. Thermal conditions which allow for fast crystallization should not be too similar to the standby conditions, e.g. room temperature. Otherwise data retention cannot be sustained. With proper activation energy for crystallization it is possible to have high speed crystallization at programming conditions while having very slow crystallization at normal conditions. Simone et al., (2008) explored material requirements for PRAM and came up with the following parameters as having a great influence on the performance of PRAM:

(i) Melting temperature - This determines the power required to RESET the cell. Melting temperature is typically determined by calorimetric measurements and is not only a function of the material composition but also a function of film thickness. This is extremely important when scaling of PRAM devices is to be considered.

(ii) Crystallization temperature - Archival lifetime and maximum operation temperature is determined by this parameter. The crystallization temperature determines the threshold switching voltage due to crystal structure-induced carrier generation. The lower the crystallization temperature the lower the threshold memory switching voltage as well as lower activation energy.

(iii) Crystallization speed - This is the data rate limiting factor. Melt quenching can be inherently very fast if a strong enough current pulse can heat the material above the melting temperature. One also needs to bear in mind that crystallization times of an actual device can be influenced by factors such as surrounding materials, the thermal properties of the cell, and the size of the cell (in particular for growth dominated materials).

(iv) Resistances in both phases - This determines the on/off ratio and also the required current to SET (crystallize) and RESET (amorphize) the cell. The resistance, in both the amorphous (R_{am}) and the crystalline (R_x) phases, are essential parameters for device functionality. The requirements are that the on/off ratio (more accurately it should be the off/on ratio because it is R_{am}/R_x) is high enough for good read margin, and it is advantageous if both resistivities are relatively high, helping to reduce the RESET current by a larger voltage drop over the phase change material (Lankhorst, 2002).

(v) Thermal conductivity - Materials with low thermal conductivity lead to more efficient heating. Even though the thermal conductivity of the phase change material has a strong influence on the thermal properties of PRAM cells, there is not much room in terms of optimization because most phase change materials have similar thermal conductivities.

(vi) Chemical stability - If phase separation or material aggregation occurs after repeated cycling, the cell performance will be influenced. Chemical reactions with the electrodes and other surrounding material will influence cell performance. Chemical stability of the phase change material is essential as the material is repeatedly melted next to electrodes and a surrounding insulator. It has been established that repeated switching can lead to phase separation in PRAM cells which, in turn, can lead to the failure of the cell.

2.2 Related studies

Tripathi *et al.,* (2010) investigated the effect of indium concentration on the electrical properties of InSe alloy. DC measurements were then made on the In_xSe_{1-x} films at all concentrations in the temperature range of 100-400K. The obtained results revealed three distinct regions. Temperature dependence of conductivity was analyzed by three mechanisms: extended state conductivity, conduction in band tails and conduction in localized sites. It was clear from the results that at high temperature conductivity mechanism obeys the law $\ln \sigma \alpha 1/T$ and at low temperatures: $\ln \sigma \alpha 1/T^{-1/4}$ indicating variable range hopping energy in the localized states near the Fermi level $N(E_f)$. They found that the incorporation of In atom in the Se matrix leads to an increase in the electrical conductivity and decrease in thermal activation energy.

Hwang *et al.* (2003) reported a higher electrical resistivity for In_2Se_3 with crystallization as compared with GST during a symposium on VLSI technology. They found that the electric resistivity of In_2Se_3 can be varied by the factor of 10^5 as compared to 10^3 for GST. Thus the switching power can be delivered more effectively due its higher resistivity.

Another advantage that has caused great interest in In_2Se_3 for phase change memory is its thermodynamic stability as reported by Vassiliev *et al.,* (1998). This coupled with the fact that In_2Se_3 is a single phase binary compound, a low melting temperature compound is not formed, and thus phase decomposition related device failure can be avoided. It was

also noted that In-Se amorphous network structure is weak; hence faster crystallization can be done.

Lee *et al.* (2005) investigated the switching behavior of indium selenide based phase-change memory cell. They performed the static mode (DC test) switching for a 5μm-sized In_2Se_3 PRAM device. In the first sweep, the as grown amorphous In_2Se_3 resistor showed high resistance state at low voltage region. However, when it reached the threshold voltage, the electrical resistance of the device drastically reduced through the formation of an electrically conducting path. The pulsed mode switching of the 5 μm-sized In_2Se_3 PRAM device showed that the reset (crystalline to amorphous) of the device was done with a 70ns-3.1V pulse and the set (amorphous to crystalline) of the device was done with 10μs-1.2V pulse. As high as 100 of switching dynamic range (ratio of R_{high} to R_{low}) was observed.

Pathan *et al*. (2003) prepared and characterized Indium Selenide thin films from a chemical route. The films were characterized by various experimental methods for structural, surface morphological, compositional, optical and electrical properties. The films were nanocrystalline and showed the phases of InSe, In_2Se_3 and In_6Se_7. The surface of the film was rough. The absorbance of the film was found to be high ($10^4 cm^{-1}$) and the optical bandgap was found to be 2.5eV. The electrical resistivity was of the order of $10^6 \Omega cm$ with n-type electrical conductivity.

Wuttig *et al.* (2002) presented a strategy to identify phase change materials with fast transformation kinetics. A microscopic investigation of crystallization kinetics in GST using a static tester and an atomic force microscope demonstrated that for different alloy compositions recrystallization proceeds via growth from the crystalline rim or by nucleation and growth of critical nuclei. Further, crystallization kinetics was drastically altered by introducing appropriate interface layers. They also suggested a possibility of optimizing transformation kinetics by applying combinatorial concepts.

Bo *et al*. (2005) fabricated a non volatile memory cell with Sb_2Te_3 chalcogenide using focused ion beam method. The thickness of the film was 40nm with contact size between the phase change film and the electrode film in the cell element being 2826nm^2. For this cell the threshold switching current of about 0.1mA was obtained. A RESET pulse width as short as 5ns and the SET pulse width as short as 22ns for the cell were obtained.

Ting *et al.* (2007) fabricated a high speed chalcogenide random access memory cell based on $Si_2Sb_2Te_5$. This cell had outstanding data retention and electrical performance. The technology adopted was the complementary metal oxide semiconductor (CMOS). The cell thickness was 0.18mm. The SET and RESET times were 31 and 10ns when the corresponding voltage pulses were 2 and 3.5V respectively. This tertiary compound possessed better data retention and lower threshold current compared to $Ge_2Sb_2Te_5$.

Kristy *et al*. (2007) designed a phase change memory device using two stacked layers of chalcogenide material, a Ge- based layer (GeTe or Ge_2Se_3), and a tin-chalcogenide layer

(SnTe or SnSe). They focused on exploring alternative materials and device structures suitable for phase change memory operation. It was observed that switching was dependent on the polarity of the potential applied to the electrode adjacent to the SnTe or SnSe layer. The presence of Sn-chalcogenide provided better adhesion of the memory layer to the electrode.

Lee *et al*. (2006) investigated the changes in the electrical conductivity occurring in a new composition of amorphous $Ge_1Se_1Te_2$ thin film for a high performance non-volatile phase change memory. A phase change random access memory device without an access transistor was successfully fabricated. The device had a much higher electrical resistivity than that of the conventional GST with its electrical resistivity being varied by a factor of 10^5 depending on the degree of crystallization. The static mode switching characteristics was tested for 100mm sized $Ge_1Se_1Te_2$. The results of the pulsed mode switching of the 20 mm-sized PRAM device showed that the RESET process of the device was accomplished with an 80ns, 8.6V pulse and the SET process of the device was accomplished with a 200ns- 4.3V pulse.

CHAPTER THREE

THEORETICAL BACKGROUND

3.1 Introduction

This chapter presents a review of selected memory technologies and their limitations, processes of memory fabrication and characterization of the memory cells. Memory structures fall into two broad categories; volatile and non-volatile.

3.2 Volatile memory

Volatile memories lose data when the power supply is switched off. They have evolved from the historical Williams Tube and Delay Line Memory to the present dynamic random access memory (DRAM) and static random access memory (SRAM). Upcoming volatile memory structures include the zero capacitor RAM (Z-RAM) and twin transistor RAM (TTRAM).

3.3 Non-Volatile memory

Due to their ability to store data even after the power supply is switched off, much research is underway to commercialize the technology behind it. So far a number of non-volatile memory structures are on the market but with limitations. Some are highlighted below.

3.3.1 Read Only Memory (ROM)

The first non-volatile floating gate memory was proposed by Kahng and Sze (1967). A conventional Metal Oxide Semiconductor Field Effect Transistor (MOSFET) was modified to include an embedded floating gate as shown in fig.3:1 below. The floating gate device looks like an n-channel MOSFET except that it has two gates: the floating gate and the control gate. The floating gate is able to store charges that were injected from the substrate through the thin tunneling oxide. The storage of charges changes the threshold voltage of the MOSFET and allows logic '0' and '1' to be represented.

A schematic of a floating gate device is represented below:

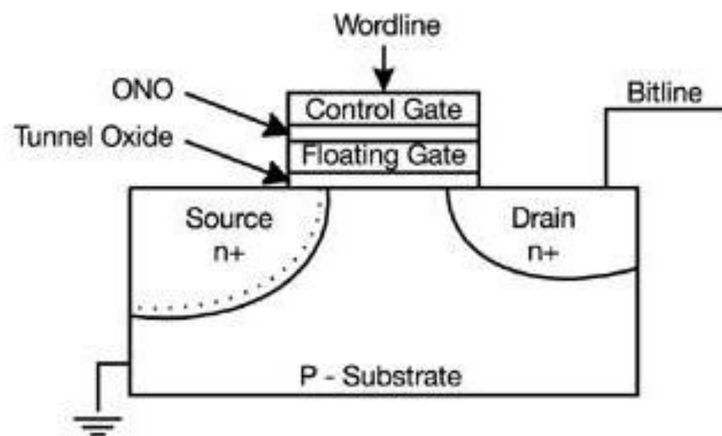

Figure 3.1: Schematic diagram of a floating gate device (www.circuitstoday.com).

3.3.2 Erasable Programmable Read Only Memory (EPROM)

A floating polysilicon gate was demonstrated by Frohman-Bentchkosky in 1970. The electrons were injected through a thick gate oxide to the floating silicon gate and

removed using ultraviolet (UV) irradiation. This was known as Erasable Programmable Read Only Memory (EPROM).

3.3.3 Electrically Erasable Programmable Read Only Memory (EEPROM)

The EEPROM utilizing tunneling write/erase was developed by Intel. Floating gate tunneling oxide (FLOTOX) technology proposed by Intel utilizes two transistors (a select transistor and a memory transistor) to achieve selective bit programming through Fowler-Nordheim (FN) tunneling. The select gate transistor is used to select or deselect floating gate transistors for programming or erase. The die size was further increased to include error correction/redundancy circuitry making them larger than EPROMs. A single transistor EEPROM cell combining hot electron programming and FN tunneling erase was introduced in the 1980s. This new generation of EEPROMs does not have the select transistor and could only be erased by resetting the devices on the entire chip or a large portion of the chip. This generally sets all bits in the block to 1. Starting with a freshly erased block, any location within that block can be programmed. However, once a bit has been set to 0, only by erasing the entire block can it be changed back to 1. This chip is the Flash EEPROM.

A smaller cell size can be achieved compared to the normal EEPROM. This can be further scaled down by using a thinner gate dielectric. However, as the gate oxide gets too thin, there will be current leakage problems, causing data retention issues. This limits the scalability of the minimum dimension of the memory cell. Conventional state of the art Flash memory stores information in floating gates transistors similar to those illustrated in figure 1 above. Traditionally, each transistor or cell holds one bit. However,

new flash systems can hold multiple bits and are called multi level cell devices. As aforementioned, information is stored inside the floating gate by trapped electrons. In a NOR flash cell, the floating gate is programmed by placing a large voltage at the control gate. Electrons are sucked up and deposited at the floating gate via a process called hot electron injection (HEI). In order to erase, a large negative voltage is supplied at the gate and the electrons tunnel out by FN-tunneling. The high voltage required is generated using an on chip charge pump. Most modern NOR flash components are divided into erase segments, usually called either blocks or sectors. All of the memory cells in block must be erased at the same time. NOR programming however, can generally be performed one byte or word at a time.

On the other hand, NAND flash memory uses tunnel injection for writing and tunnel release for erasing. In NOR cells, the source or drain of the transistor are connected to single bitline in parallel. In NAND cells, the memory cells are connected from a single bitline in series. The wordline connected to the control and floating gate, is staked above the silicon substrate. Adjacent transistors share the same source/drain. The parallel configuration of NOR Flash enables random access of data enabling fast read speed. Hence NOR flash is ideal for applications which are frequent read only or perform read operations such as code storage. NAND Flash enjoys higher cell density for a given technology node. This translates to smaller chip size, lower cost per bit and faster read/write/erase speed through programming blocks of data. Hence, NAND is ideal for applications such as data storage which requires low cost, small size and which rewrites data frequently. Great efforts have been carried out to make Flash memory cells smaller

and more portable and the same time faster and with lower power consumption. However, there is a limit to which cell size can be scaled down. Current flash memory technology is expected to be replaced or undergo some radical changes in the not-so distant future. There has been intense research interest into the various options available and new technologies have been mooted as potential successors to conventional flash technology. The major forerunners are briefly discussed below.

3.3.4 Silicon Oxide Nitride Oxide Semiconductor (SONOS)

SONOS cells consist of a standard n-channel MOS transistor with additional layers of insulators on the gate. These include the oxide layer (~ 2 nm), a silicon nitride layer (~ 5nm) and a second oxide layer (5-10 nm). SONOS is similar to flash memory. However, it relies on charge trapping mechanism in which electrons are trapped in the nitride layer. SONOS offers a lower power usage, improved cycling endurance, reduction in process complexity and elimination of drain induced turn on. The SONOS memory device is more scalable than the floating gate flash memory device since the equivalent oxide thickness (EOT) of the gate stack is thinner in the SONOS memory than in the floating gate memory. Moreover, current manufacturing process are simpler compared to flash manufacturing processes as they only require four additional non critical masking steps over the basic logic processes (flash floating gate requires eleven additional processes). Also the trapped nitrides do not leak away easily and hence SONOS are more radiation hard than conventional flash whose thin tunneling oxide is easily damaged by large ionizing doses, leading to charge leakage.

3.3.5 Ferroelectric Random Access Memory (FeRAM)

A ferroelectric memory cell consists of a ferroelectric capacitor and a MOS transistor. It is similar to the storage cell of a DRAM. However, the material between the capacitor's electrodes has a high dielectric constant and can be polarized by an electric field. When an external electric field is applied across a dielectric the dipoles tend to align themselves with the field direction as a result of small shifts in the positions of the atoms and shifts in the distributions of electronic charge in the crystal structure. The polarization remains even when the electric field is removed and remains until it gets reversed by an opposite electrical field. This makes the memory non-volatile. The polarity and quality of stored data is dependent on the direction and strength of the remnant polarization after the electric field is removed. Ferroelectric memories can be written much faster than EEPROMs and operating voltages are relatively small. FeRAM is also radiation hard. Today's FeRAM uses lead zirconate titanate (PZT); other materials are being considered. FeRAM is a development of Ramtron International.

The main set back of FeRAM is incorporating ferroelectric materials into the current silicon manufacturing processes. The International Technology Roadmap for Semiconductors (ITRS) also highlighted that continued scaling of the stack capacitor would be challenging and FeRAM production is sensitive to processing conditions and temperature.

3.3.6 Magnetic Random Access Memory (MRAM)

In MRAM the information is stored as the magnetization direction of ferromagnetic elements. In MRAM, the elements are formed from two ferromagnetic plates each of which can hold a magnetic field, separated by a thin insulating layer. It utilizes the tunneling magnetoresistive (TMR) effect. The tunneling energy for the electrons that are spin aligned with both magnetic layers is less than that for electrons that are spin aligned with only one layer. When the orientation of both magnetic layers is the same, the spin aligned electrons have a higher probability of tunneling through the insulating layer. When the magnetic orientations of the layers are opposite, the tunneling probability of both spin up and spin down electrons is reduced. Due the magnetic tunnel effect, the electrical resistance of the cell changes depending on the orientation of the fields in the two plates. Two plates having the same polarity indicates a logic state of “0”, while two plates of opposite polarity indicate a logic state of “1” as resistance is higher.

Another type of MRAM consists of two ferromagnetic plates separated by a magnetic, non metallic spacer layer. This utilizes the giant magnetoresistive (GMR) effect. Free electrons are generated spin up and spin down in equal proportions. When the orientations of magnetic layers are parallel, only one type of electron is retarded. When the magnetic orientations of the layers are antiparallel, both spin up and spin down electrons suffer retardation. In this way, resistance is varied to give logic “0” and “1”. For both methods one of the two plates is commonly fixed to one polarity and the others field will change to match that of an external field. Issues with future development of MRAM

include disturbances from neighboring cells, stability issues concerning the tunneling barrier and the free layer with increased scaling.

3.3.7 Nanocrystal Memory (NC)

Another area of active research is the use of nanocrystals to replace a single floating gate as storage sites. This is similar to the use of nitride traps in SONOS memory. Among the advantages of this technology are that it is easy to integrate nanocrystal memories into current CMOS processes, easy to scale, low read/write voltages and the requirement of only 4 mask adders to the baseline CMOS manufacturing process unlike the 11 for conventional flash memories. The weakness of this memory structure is the low write/erase speed and low endurance compared to the competitors like MRAM and PRAM

3.3.8 Phase Change Random Access Memory (PRAM)

PRAM makes use of the reversible phase transition of chalcogenide-based materials; the data is stored as crystalline states of the chalcogenide resistor. The basic switching mechanism of PRAM can be explained in terms of phase transition between amorphous and crystalline states as follows. The crystalline state of the chalcogenide material is controlled by means of an electric pulse (Lai *et al.,* 2001). Using a high voltage and a short duration pulse, the phase change resistor is heated up to its melting temperature and then quenched. In this way the phase of the chalcogenide becomes amorphous and develops high electrical resistance. The phase change (PC) resistor with an amorphized

region is then returned to the crystalline phase using a low voltage and relatively long duration pulse. Due to the low voltage pulse, the temperature of the phase change resistor is increased, but cannot reach to the melting temperature. When the phase change resistor with an amorphized region is heated, nucleation and growth of crystalline phase and amorphous region becomes crystalline phase. Thus, the electrical resistance of resistor is also returned. The switching requires relatively large current to heat up the phase change resistor and to create thermally induced transition. Since the electric resistivity of the amorphous chalcogenide is orders of magnitude higher than that of crystalline chalcogenide, phase transition of chalcogenide transistor can easily be sensed by applying the low bias voltage. The dramatic differences in the electric resistivity of amorphous and crystalline states of chalcogenide based materials forms the basis by which data are stored. The amorphous high resistance state is used to represent a binary 0, and the crystalline, low resistance state represents a 1. Figure 3.2 shows a cross section of a PRAM test device.

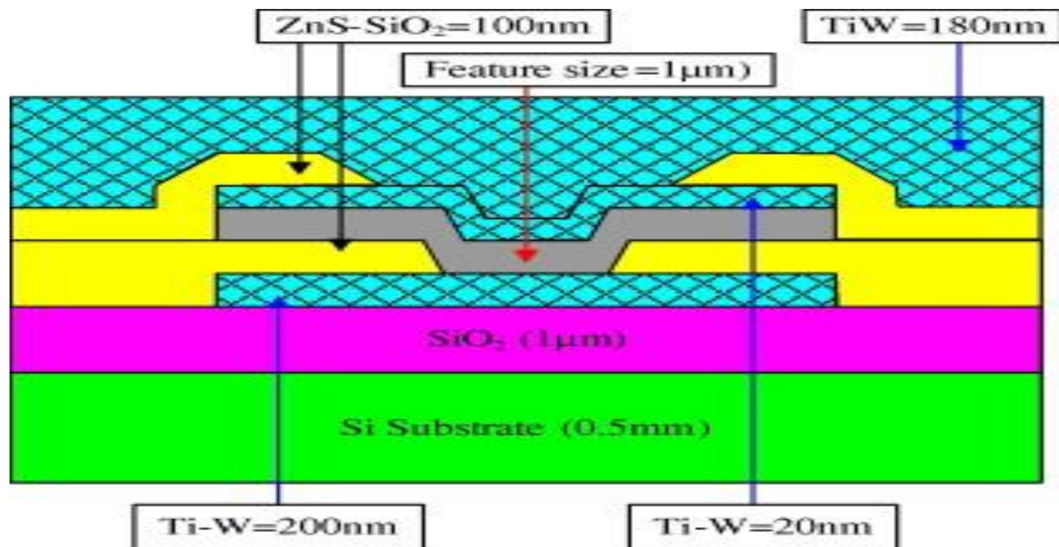

Figure 3.2: A schematic diagram of the cross-sectional view of PRAM cell structure (Lee *et al*., 2005)

Issues at hand for this technology include: data retention, thermal cross talk, cyclic endurance and polarity. Table 3.1 compares some of the key attributes of PCM with other memory structures. Care has to taken in making comparisons since some of the memory structures such as MRAM and nanocrystal memories are manufactured based on older technology nodes compared to conventional flash. Others such as PCM have not been mass manufactured at the time of writing and performances can only be compared based on research papers and press releases.

Table 3.1: A summary of the various memory technologies and their attributes (Kian, 2006)

Memory Type	**Flash NOR**	**Flash NAND**	**FeRAM**	**MRAM**	**PRAM**	**SONOS**	**NC Memory**
Endurance	1.0E+5	1.0E+5	1.0E+13	>3.0E+16	1.0E+12	1.0E+7	1.0E+7
Data Retention	20	20	10	>10	>10	20	20
Read/Program voltage(V)	2/10	2/18	1.5/1.5	3.3/3.3	0.4/1	2/5.5	1/6
Read Time per Bit	Fast ~10ns	Fast ~50ns	Fast 30-60ns	Fast 5-70ns	Medium 70ns	Fast	Fast
Write Time per Bit	Low ~2ms	Low 0.4ms	Medium 30-60ns	Fast 5-70ns	Medium 100-500ns	Low/medium 10μs	Medium <10μs
Erase Time per Bit	Low 100ms	Medium, 2ms	Medium 30-60ns	Fast 5-70ns	Medium 100-500ns	Medium ~1ms	Low/Medium <100ms
Mask Adders to CMOS logic	11	11	2	3	5	4-7	4
Process Technology	Charge Tunneling	Charge tunneling	Ferro-electri	Magnetization	Phase transition	Charge tunneling	Charge tunneling

3.4 Thin film Deposition

Film deposition involves controlled transfer of atoms from a source to a substrate where film growth and formation takes place atomistically (Ohring, 1992).

3.4.1 Theory of crystallization

3.4.1.1 Nucleation and crystal growth in chalcogenide glasses

The crystallization process is in general a nucleation and growth transformation (Lee *et al.,* 2005; Raoux *et al.,* 2009; Heireche and Belhadji (2007). Depending on the material, one or the other of these processes dominates the progress of crystallization. Nucleation can occur in the interior of the amorphous material (homogeneous nucleation) or at the interface of the amorphous material (heterogeneous nucleation) with the substrate, at the interface with the capping layer (if present), or at the sample surface which in practical cases will be a thin oxide layer unless the sample is prepared and crystallized in situ (Raoux 2009). In addition, for PCMs, the crystallization is assumed to be diffusion limited (as opposed to collision limited) because atoms jump by diffusion over the amorphous –crystal boundary. The final steady-state nucleation rate I^{ss} is given by

$$I^{ss} = S_C \cdot \frac{2K_B T}{\eta \pi a^2} \cdot N_0 \cdot \Gamma_z \cdot \exp\left(-\frac{\Delta G_C}{K_B T}\right), \tag{3.1}$$

where s_c is the number of surface atoms in a critical cluster, k_B is the Boltzmann constant, N_0 is the total number of atoms in the amorphous phase per unit volume, ΔG_c is the reversible work for cluster formation at the critical radius, η is the liquid shear velocity, a is the average inter-atomic distance, T is temperature and Γ_z is a pre-factor called Zeldovich factor (Raoux, 2009). For PCMs the nucleation rate shows a maximum between the glass transition temperature and the melting temperature.

Once the stable nuclei have formed, crystallization proceeds by growth from the crystal front. For PCMs, this process is interface controlled and independent of time. The growth velocity is proportional to diffusivity because growth occurs by diffusive jumps of atoms

over the amorphous-crystal boundary. The growth velocity is strongly temperature dependent and also has a maximum at temperature between the glass transition and melting temperature (Kalb, 2008).

PCMs can be categorized into nucleated-dominated and growth dominated materials. For nucleated dominated materials, many nuclei are formed in a unit volume; these nuclei grow relatively slowly. Critical nuclei formation also occurs continuously during the growth process so that crystals of different sizes are formed (Kalb *et al.,* 2004). For growth dominated materials, very few critical nuclei are formed after an often relatively long incubation time, but then crystallization occurs by rapid growth. For these materials, the crystals have similar sizes (Kalb *et al.,* 2004). To distinguish between nucleation dominated material and growth dominated materials, recrystallization times of melt-quenched amorphous spot in a crystalline film as a function of spot size, was measured by the group Raoux *et al* (2008). It was determined that if the crystallization speed depends on the spot size, crystallization proceeds mainly from the crystalline amorphous border and the material is growth dominated. However, if the crystallization speed does not depend on the spot size, crystallization occurs mainly by the formation of new crystals and the material is nucleation dominated.

For many technical applications, the dominant nucleation process is not homogenous but heterogeneous nucleation. The surrounding of the PCM plays an important role and nucleation often occurs at interfaces. The heterogeneous nucleation rate can be many orders of magnitude larger than the homogenous nucleation rate (Raoux *et al.,* 2009), and

in most PCM devices, there is an interface present between the amorphous material and crystalline material, so nucleation is not even needed for crystallization (Kalb *et al.,* 2004). Static laser tester experiments have found that melt-quenched, amorphous materials can have crystallization times that are orders of magnitude shorter than those for as-deposited, amorphous materials (Raoux *et al.,* 2009). This is due to the above mentioned existence of an amorphous-crystalline interface for melt-quenched material in these experiments.

Archival lifetime is important for the vitality of a data storage technology. For phase change technologies, archival lifetime means the stability of the amorphous area against crystallization for long times and often at elevated temperatures. This property is of phenomenal significance and is related to the crystallization temperature. Materials with higher crystallization temperatures often have a better thermal stability. In optical storage, the archival lifetime is measured as the change in reflectivity of an amorphous mark in a crystalline disc. In PCM it is determined by the change in resistivity of the Reset (amorphized) cell over time.

Several factors contribute to nucleation and growth kinetics: temperature (Kalb *et al.,* 2005), composition (Coombs *et al.,* 1995; Lankhorst *et al.,* 2005; Wuttig *et al.,* 2002), Material interfaces (Ohshima, 1996), device geometry (Lankhorst *et al.,* 2005; Wu *et al.,* 2008), device size (Wang *et al.,* 2008), material thickness (Raoux *et al.,* 2008) and device history (Coombs *et al.,* 1995; Raoux *et al.,* 2008). Of these, the two most important factors governing switching speeds are temperature and local composition. In fact, it has

been reported that most of the macroscopically observable nucleation effects associated with geometry, size, thickness, device history and material interfaces can be understood in terms of varying local composition on the delicate balance between surface and volume energies that drive crystallization (Burr *et al.,* 2010).

3.4.1.2 Thermal analysis

Thermal analysis has been used in the study of crystallization kinetics of glasses. There exist two thermal analysis methods: One is the isothermal method known as Johnson-Mehl-Avrami (JMA) in which glass samples are quickly heated up and held at a temperature above glass transition temperature, and the other method is the constant heating rate known as the Kissinger method (Heireche and Belhadji, 2007; Cheng, 2001). The disadvantage of isothermal method is in reaching the required temperature instantaneously and taking the readings at that point (Rao *et al*., 2008). The parameters usually discussed are the activation energy, the index η (known as the Avrami exponent) and the pre-exponential frequency factor. The crystallization process as has been discussed is a nucleation and growth transformation. In principle, given sufficient time, this transformation continues until complete. Although the degree of transformation does not depend on temperature, the velocity of transformation is strongly dependent temperature. The JMA transformation equation relates the fraction of material transformed with time at constant temperature. The arguments used in this derivation are largely independent of models used to describe the mechanism of transformation. If a homogeneous reaction is assumed, the probability of transformation in any small region in a given time interval will be the same for all such regions in the untransformed

volume. Therefore, the volume transformed in an infinitesimal time interval will be proportional to the volume remaining untransformed at the beginning of the time interval. This in effect leads to a first order rate process. Taking the total volume as V_o and the volume transformed in time *dt* as V, then the transformation could be expressed as

$$\frac{dV}{dt} = k(V_o\text{-}V) \tag{3.2}$$

Leading to

$$\frac{V}{V_0} = \alpha(t) = 1 - \exp(-kt) \tag{3.3}$$

where k is known as the rate constant and α(t) is the fraction of material transformed after a time *t*. Equation (3.3) was derived assuming a homogeneous reaction at constant temperature. However, the situation is more complex for nucleation and growth reactions. Such considerations are incorporated into the JMA equation which is given by

$$\alpha(t) = 1 - \exp\left[-k(t - t_0)^n\right] \tag{3.4}$$

where t_o is the incubation time and the exponent $n = n_n + n_g$ with $4 \geq n \geq 1.5$ can be related to growth mechanisms. When $0 < n_n < 1$, the process is said to be nucleated dominated and when $4 \geq n_g \geq 1.5$, the growth mechanisms dominates. *k* is usually found to follow an Arrhenius-type equation of the form

$$k = k_o exp[-\frac{\Delta E}{k_B T}] \tag{3.5}$$

where k_o is a pre-exponential frequency factor. Combining Equations (3.4) and (3.5), one gets

$$\ln\{-\ln[1-\alpha(t)]\} = \ln k + n\ln(t-t_o), \tag{3.6}$$

Therefore a plot of $\ln\{-\ln[1-\alpha(t)]\}$ versus $\ln(t-t_o)$ at constant temperature will give a straight line with slope *n* and intercept ln*k*. Eq. (3.6) could be arranged to read as

$$\ln k = \ln k_0 - \frac{\Delta E}{k_B T} \tag{3.7}$$

Thus by obtaining a series of values for ln*k* at different T, we are able to find ΔE and K_o.

For the Kissinger method, a first-order rate process is given by

$$\frac{\partial x}{\partial t} = k(1-x)_T \tag{3.8}$$

Without loss of generality, *k* is defined by eq. (3.5). For time independent temperature changes,

$$\frac{dx}{dt} = \left[\frac{\partial x}{\partial t}\right]_T \tag{3.9}$$

After combining eq. (3.29) and (3.30), the following expression is obtained:

$$\frac{d}{dt}\left[\frac{\partial x}{\partial t}\right] = \left[\frac{\Delta E}{k_B}\frac{dT}{dt} - k_0 \exp\left[-\frac{\Delta E}{k_B T}\right]\right]\frac{\partial x}{\partial t} \tag{3.10}$$

`

The requirement that the left hand side of the eq. (3.10) should vanish for an exothermic or endothermic peak gives

$$\ln\left[\frac{\beta}{T_p{}^2}\right] = -\frac{\Delta E}{k_B}\left[\frac{1}{T_p}\right] + const, \tag{3.11}$$

where T_p corresponds to the peak temperature and $\beta = \frac{dT}{dt}$ = rate of heating. If a plot of $\ln\left[\frac{\beta}{T_p^2}\right]$ versus $\frac{1}{T_p}$ gives a straight line, then its slope yields ($-\frac{\Delta E}{k_B}$), from which ΔE is easily determined. (Cheng, 2001).

A number of practical deposition techniques exist and are classified into two broad categories i.e. the physical vapor deposition (PVD) and chemical vapor deposition (CVD). Each is discussed below with its variants.

3.4.2. Chemical Vapor Deposition (CVD)

Chemical Vapor Deposition techniques include; vapor phase epitaxy (VPE), metal oxide chemical vapor deposition (MOCVD), molecular beam epitaxy (MBE), and liquid vapor epitaxy (LVE) among others.

3.4.2.1. Liquid Vapor Epitaxy (LVE)

This technique involves the precipitation of a crystalline film from a supersaturated melt onto a parent substrate, which serves as both the template for epitaxy and the physical support for the heterostructure. A detailed analysis of LVE is extremely complicated in ternary systems because it requires knowledge of the thermodynamic equilibria between solids and solutions, nucleation and interface attachment kinetics, solute partitioning, diffusion, and heat transfer. LVE however, offers several advantages over other epitaxial deposition methods, including low cost apparatus capable of yielding films of controlled composition and thickness, with lower dislocation densities than the parent substrates. Limitations of LVE include poor thickness uniformity and rough surface morphology particularly in thin layers.

3.4.2.2. Vapor Phase Epitaxy (VPE)

This has widely been used with two novel concepts emerging in the recent past. The first is vapor levitation epitaxy (VLE). Here, the heated substrate is levitated above a nitrogen track close to a porous frit through which the hot gaseous reactants pass. Upon impingement on the substrate, chemical reactions and film deposition occur while the product gases escape into the effluent stream (Ohring, 1992). The VLE process was designed for the growth of epitaxial III-V semiconductor films and several advantages worth noting:

(i) There is no physical contact between substrate and reactor.

(ii) Thin layer growth is possible.

(iii) Sharp transitions can be produced between film layers of multiple stacks.

(iv) Commercial scale-up appears to be feasible.

The second method, known as the rapid thermal CVD processing (RTCVD), is an elaboration on conventional VPE. Epitaxial deposition is influenced through rapid, controlled variations of substrate temperature. Source gases react on low-thermal-mass substrates heated by the radiation from external high intensity lamps. The later enable rapid temperature excursions and heating rates of hundreds of degrees Celsius per second are possible. For group III-V semiconductors, high quality epitaxial films have been deposited by first desorbing substrate impurities at elevated temperatures followed by immediate lower temperature growth (Green, 1989). Very high quality lattice-matched heteroepitaxial films can be grown by VD methods. This is particularly true of organometallic vapor phase epitaxy (OMVPE) techniques where atomistically abrupt

heterojunction interfaces have been demonstrated in alternating AlAs-GaAs (superlattice) structures.

3.4.2.3. Molecular Beam Epitaxy (MBE)

Molecular-Beam Epitaxy is conceptually a rather simple single crystal film technique that however, represents the state of the art attainable in deposition processing from the vapor phase. It essentially involves highly controlled evaporation in an ultra-vacuum (~ 10^{-10}torr) system. Interaction of one or more evaporated beams of atoms or molecules with the single crystal substrate yields the desired epitaxial film. The clean environment coupled with the slow growth rate and independent control of the beam sources enables the precise fabrication of semiconductor heterostructures at an atomic level. Deposition of thin film layers from a fraction of a micron thick down to single monolayer is possible. In general, MBE growth rates are quite low, and for GaAs materials a value of 1µm|h is typical. A modern MBE system typically is very expensive (~ more than 1 million US dollars). Arrayed around the substrate are semiconductor and dopant sources, which usually consist of so-called effusion cells or electron-beam guns. The later is used for high melting Si and Ge materials. On the other hand, effusion cells consisting of an isothermal cavity with a hole through which the evaporant exits are used for compound semiconductor elements and their dopants. Effusion cells behave like small-area sources and exhibit a cos Φ emission. A recent advance in MBE technology incorporates a gas source to supply As and P. Organometallics used for this purpose are thermally cracked, releasing the group V element as a molecular beam into the system. Excellent epitaxial

films quality has been obtained by this hybrid MBE-OMVPE process, which is known by the acronym MOMBE.

3.4.3. Physical Vapor Deposition (PVD)

In PVD, the main techniques used as mentioned earlier are sputtering and evaporation and are briefly discussed below.

3.4.3.1 Sputtering

In this technique, fast moving and energetic ions bombard a target ejecting some atoms from its surface. The figure 3.3 show how the ejected atoms impinge on a substrate (anode) forming a thin film coating on a substrate within the deposition chamber.

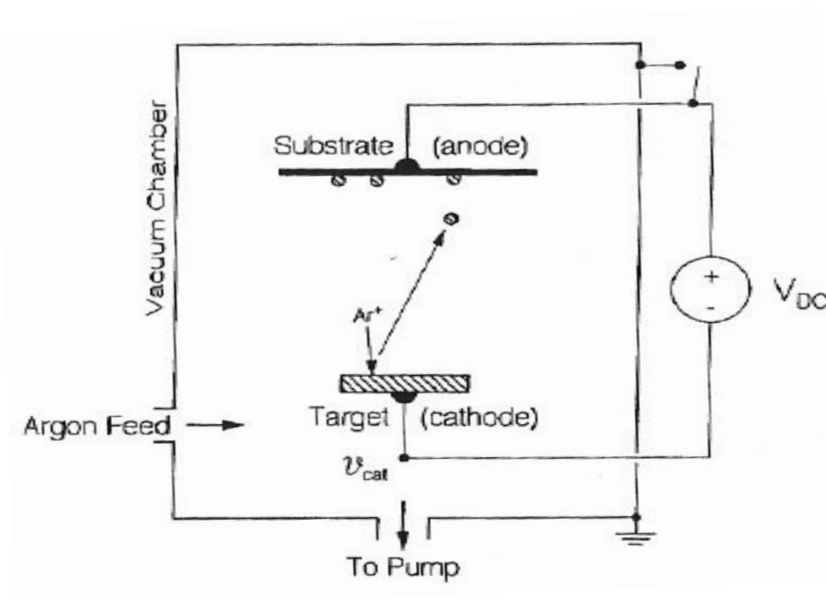

Figure 3.3: Schematic illustration of DC magnetron sputtering process which utilizes dc gaseous exchange (Ohring, 1992).

Argon gas is often used as a sputtering gas. DC sputtering uses high potential difference between anode substrate and cathode target that accelerates the ejected atoms towards the substrate forming a film (Ohring, 1992). There are four types of sputtering techniques that are commonly used. They include; DC Sputtering, RF Sputtering, Magnetron and Reactive sputtering. There are also important variants within each category for example DC bias and even hybrids between categories (Almen and Bruce, 1961). RF sputtering is mainly used for making dielectric (non conducting) films whereas DC Magnetron sputtering is used for depositing conducting and doped semiconductor films. DC Magnetron sputtering is presently the most widely commercially used method due to its high deposition rates (Ohring, 1992).

3.4.3.2 Evaporation

There are many techniques employed under evaporation for epitaxial film growth. Among them are: co-evaporation, flash evaporation, and single source evaporation. Usually the sample is placed on evaporator boats which are heated above the melting points of the elements until they vaporize and deposit on a substrate above the boat at a lower temperature. Co-evaporation is single stage growth technique which is complex requiring accurate control of all evaporation sources. Flash evaporation on the other hand, suffers from inherent problems such as poor reproducibility, inferior crystallinity and spitting of materials from evaporation boats. In this study, chalcogenide thin films were prepared by single source evaporation. The schematic illustration of single source evaporation is as shown in figure 3.4.

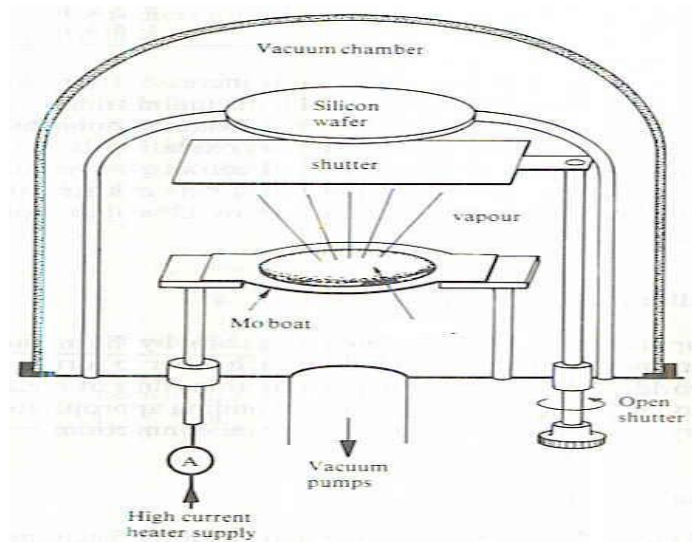

Figure 3.4: Schematic diagram of vacuum evaporation process for metallization (Anderson *et al.,* 1985).

Here, predetermined masses of pulverized chalcogenide In_xSe_y was placed directly on a single unheated evaporation boat at room temperature followed by controlled increase in boat temperature under high vacuum conditions. This way, material spitting will be prevented, device quality material will be produced and compositional uniformity over large areas is guaranteed. Until the late 1960s, evaporation clearly surpassed sputtering as the preferred film deposition technique. Higher deposition rates, better vacuum and thus cleaner environment for film formation and growth, and general applicability to all classes of materials were some of the reasons for the ascendancy of evaporation methods. However, films used for magnetic and microelectronic applications necessitated the use of alloys, with stringent stoichiometry limits, which had to conformally cover and adhere well to substrate surfaces. These demands plus the introduction of radio frequency (RF), bias, and magnetron variants, which extended the capabilities of sputtering, and the availability of high purity targets and working gases, helped to promote the popularity of

sputter deposition. In many instances, features of both have been forged into hybrid processes.

Based on experimentation on the evaporation of mercury, it was observed that evaporation rates were:

(i) Not limited by insufficient heat supplied to the surface of the molten evaporant.

(ii) Proportional to the difference between the equilibrium pressure P_e of the Hg at the given temperature and the hydrostatic pressure P_h acting on the evaporant.

Hertz concluded that a liquid has a specific ability to evaporate at a given temperature. Furthermore, the maximum evaporation rate is attained when the number of vapor molecules emitted corresponds to that required to exert the equilibrium vapor pressure while none return. These ideas led to the basic equation for the rate of evaporation from both liquid and solid surfaces, namely,

$$\Phi_e = \frac{\alpha_e N_A (P_e - P_h)}{\sqrt{2\pi MRT}} \quad (3.12)$$

Where **Φe** is the evaporation flux in number of atoms or molecules per unit area per unit time, and α_e is the coefficient of evaporation, which has a value between 0 and 1. When $\alpha_e=1$ and P_h is zero, the maximum evaporation rate is realized. An expression for the maximum value of Φe would be

$$\Phi_e = 3.513x10^{22} \frac{P_e}{\sqrt{MT}} molecules / cm^2 - Sec. \quad (3.13)$$

When P_e is expressed in torr, a useful variant of this formula is

$$\Gamma_e = 5.83x10^{-2} \sqrt{\frac{M}{T}} P_e g / cm^2 - Sec. \quad (3.14)$$

where r_e, is the mass evaporation rate. At a pressure of 10^{-2} torr, a typical value of r_e for many elements is approximately10^{-4}g/cm^2-sec of evaporant. The key variable influencing evaporation rates is the temperature, which has a profound effect on the equilibrium vapor pressure. In the next section, a brief theory of thin film optics is presented. (Hertz, 1882)

3.5 Optical characterization

Optical spectra of semiconductor films provide information on their electronic characteristics. Once photons are incident on a film, they interact with electrons of the films. A photon may be reflected, transmitted, scattered or undergo luminescence.

3.5.1 Optical Reflectance

Reflectance is the percentage measure of the ratio of intensity of incident light shone onto the surface of the film and the intensity of reflected light measured. The two intensities are compared by a quantity referred to as the reflectance (R) given in equation 3.15.

$$R = \frac{I_R}{I_O} \times 100 \tag{3.15}$$

where R is the reflectance, I_R the reflected intensity and I_O the incident intensity.

3.5.2 Optical transmission

Photons of selected wavelengths and beam intensity (photons/cm^2-s) are directed at the film. Those photons with energies greater than the band gap (E_g) are absorbed while those with energies less than band gap are transmitted. This is because photons with

energy less than band gap do not excite electrons in the valence band to higher states, hence transmitted. The ratio of the intensities of incident photons (I_o) to the transmitted photons (I_t) is a measure of the transmittance of a given material. This can be expressed as in equation 3.5 below.

$$T = \frac{I_t}{I_o} \tag{3.16}$$

3.5.3 Absorption of light

Absorption takes place when a photon of energy more than the band gap excites an electron from lower energy state. Figure 3.5 show how light incident on a thin film is absorbed.

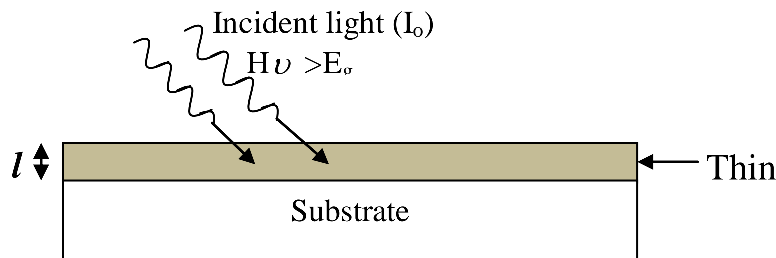

Figure 3.5: Schematic representation of the Interaction of light with the thin film.

Absorption is expressed by absorption coefficient (α) which is the relative rate of decrease in light intensity along the propagation path. Absorption coefficient is expressed by Beer's law given by equations 3.16 and 3.17

$$\mathbf{I_t = I_O e^{-\alpha l}} \tag{3.17}$$

$$\alpha = \frac{1}{l} \ln\left(\frac{I_O}{I_t}\right) \tag{3.18}$$

Where I_t is transmitted intensity, Io incident intensity, α is the absorption coefficient and l the film thickness.

Amount of absorption depends on photon wavelength, film thickness and film properties. Absorption coefficient is zero or very small for photon energies below band gap and well above phonon energies. As photon energy is increased beyond band gap, absorption coefficient increases rapidly to values larger than $10^4 cm^{-1}$. This makes them opaque for photon energies higher than band gap unless thickness is very small (Yu and Cardona, 1996). Absorption coefficient is related to frequency (ω) and extinction coefficient (k) by equation 3.19 below (Wooten, 1972).

$$\alpha = \frac{2\omega k}{c} = \frac{4\pi k}{\lambda} \tag{3.19}$$

3.5.4 Dielectric function (ε)

Dielectric is a dimensionless property of a material associated with its permittivity. Permittivity is a measure of the ability of a material to be polarized by an electric field. Dielectric function is frequency dependent property of thin films. It is expressed as a complex dielectric function with both real (ε_1) and imaginary parts (ε_2) as given in equation 3.20 below.

$$\varepsilon = \varepsilon_1 + i\varepsilon_2 \tag{3.20}$$

In terms of refractive index (n) and extinction coefficient (k), real and imaginary parts of dielectric function are expressed in equation 3.21 and 3.22 below.

$$\varepsilon_1 = n^2 - k^2 \tag{3.21}$$

$$\varepsilon_2 = 2nk \tag{3.22}$$

Frequency dependence of dielectric constant (ε_1 and ε_2) has great influence on optical properties of thin films. This dependence can tell if a film is reflecting, transmitting, or absorbing. Reflectivity of films at normal incidence is given by the equation 3.23 (Wooten, 1972).

$$R = \frac{(n-1)^2 + k^2}{(n+1)^2 + k^2} \tag{3.23}$$

For non-magnetic materials, n and k are given by equations 3.24 and 3.25 (Wooten, 1972).

$$n = \left\{ \frac{1}{2} \left[\varepsilon_1{}^2 + \varepsilon_2{}^2 \right]^{1/2} + \varepsilon_1 \right\}^{1/2} \tag{3.24}$$

$$k = \left\{ \frac{1}{2} \left[\varepsilon_1{}^2 + \varepsilon_2{}^2 \right]^{1/2} - \varepsilon_1 \right\}^{1/2} \tag{3.25}$$

Using equations 3.24 and 3.25, reflecting, absorbing, and transparent properties of a film can be determined. In a region where $\varepsilon_2=2nk=0$ and $\varepsilon_2=n^2-k^2>1$, transparency is very high

with no absorption. However, there is little reflectivity in case of insulators (Wooten, 1972).

In spectral plots of n and k against energy (hυ) for thin films, the nature of the graph depends on the film whether it is highly transmitting or reflecting. In a region where it is transmitting, n increases as k decreases with energy. Strong absorption only takes in the neighborhood of transition frequency (frequency corresponding to a peak in the graph or frequency at which n or k is maximum). The ε_1 also depends on band gap where it decreases with increasing band gap (Wooten, 1972).

3.5.5 Refractive Index n

Refractive index is related to wave vector (k) as shown in equation 3.26 below.

$$k = \frac{\hat{n}\omega}{c} \tag{3.26}$$

Where $\hat{n}$ the complex refractive index, k is is the extinction coefficient and c the velocity of the radiation. Refractive index is also related to dispersion and absorption of radiation by the medium as given in equation 3.27.

$$\hat{n}\omega = n + ik \tag{3.27}$$

Dielectric function is directly related to numerical properties and is connected to the refractive index as follows:

$$\varepsilon = \varepsilon_1 + i\varepsilon_2 \tag{3.28}$$

$$\varepsilon_1 = n^2 + k^2 \tag{3.29}$$

$$\varepsilon_2 = 2nk \tag{3.30}$$

where ε_1 and ε_2 are respectively the real and imaginary parts of dielectric function ε, n is refractive index and k is extinction coefficient.

3.5.6 Optical penetration depth (δ)

Optical penetration depth is the depth inside a material to which a radiation penetrates before its intensity reduces to 1/e of its initial intensity. It is expressed as reciprocal of absorption coefficient. Since absorption coefficient increase with photon energy above band gap, thinner films are necessary for determination of optical constants over a wide range of photon energy (Yu and Cardona, 1996). When a wave propagates in a medium, it suffers exponential decay over a distance called optical penetration depth or optical skin depth given by equation 3.31.

$$\delta = \frac{c}{2\omega k} = \frac{\lambda}{4\pi k} \tag{3.31}$$

k is imaginary part of complex refractive index, also called the extinction coefficient.

3.5.7 Determination of band gap (E_g)

The graphical method is one of the techniques used to determine the band gap of semiconductor thin films from a plot of α^2 versus energy for the case of a direct band gap material. A straight or near straight line obtained shows that a film has a direct band gap. From figure 3.4, the spectral plot of a thin film establishes that it has a direct band gap.

The straight line is extrapolated to x-axis where the band gap is the value of energy where α=0 (Palik, 1985).

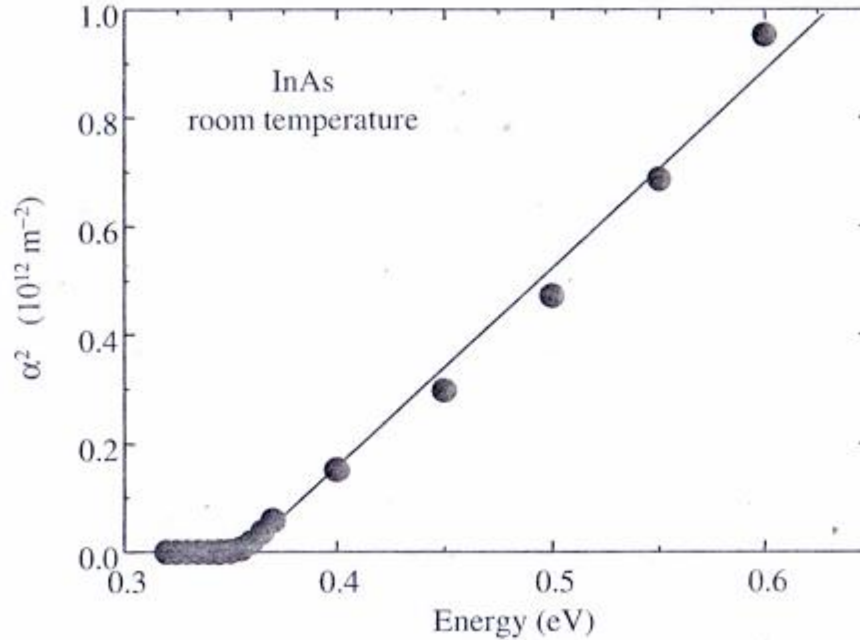

Figure 3.4: Graphical determination of band gap energies (Palik, 1985).

The band gaps of the semiconductor films are determined from spectral plot of the square of absorption coefficient versus photon energy. Absorbance has an exponential decay with increase in wavelength. This is because the photon energy is less than the bandgap hence no excitation of electron in valence band to cross to conduction band. Absorption coefficient (α) is related to photon energy (hυ) according to equations 3.32 (Ndukwe, 1998) and 3.33 (Ndukwe, 1996).

$$\alpha = \frac{(h\nu - E_g)^{1/2}}{h\nu} \tag{3.32}$$

Rearranging equation 3.32 leads to:

$$(\alpha h\nu)^2 = h\nu - E_g \quad (3.33)$$

Where h is Planck's constant (6.62×10^{-34} Js) and ν is frequency of incident photon (Eya *et al*., 2005).

3.6 Electrical Characterization

3.6.1 Electrical resistivity of Semiconductors

Electrical resistivity between metals and semiconductors vary greatly. However, a fundamental difference between a metal and a semiconductor is that the former is unipolar whereas the later is bipolar. One carrier has a negative charge (free electron) of mobility μ_n and the other has a positive charge (the hole), of mobility, μ_p. When these particles are subjected to an external electric field E, they would drift in opposite directions, but since the current of each is in the same direction, their current density J, is given by equation3.34 (Owade, 1998)

$$J = (n\mu_n + p\ \mu_p)\,\mathrm{q} = \sigma E \quad (3.34)$$

Where n is the concentration of free electrons, p is the concentration of holes, σ is the conductivity, and q is charge of the carrier.

Therefore,

$$\sigma = (\mathrm{n}\,\mu_n + p\mu_p)q \quad (3.35)$$

It is found from Fermi-function and density of states calculations that the number of electrons per unit volume

$$n = N_C e^{(\mu - E_g)/K_B T} \quad (3.36)$$

while the number of holes per unit volume is

$$p = N_V \, e^{-\mu / k_B T} \tag{3.37}$$

where N_C is effective number of levels per unit volume in conduction band, N_v is effective number of levels per unit volume in the valence band, E_G is band gap energy, k_B Boltzmann constant and μ Mobility.

Combining equations in n and p we obtain

$$np = N_c N_v e^{-E_G / k_B T} \tag{3.38}$$

The result is a function of temperature only and is independent of impurity concentration.

For a pure semi-conductor

$$\text{n=p=} (N_c N_v)^{\frac{1}{2}} e^{-E_G / 2k_B T} \tag{3.39}$$

But $\sigma = (n\mu_n + p\mu_p)q$. Thus for a pure semiconductor, σ becomes

$$\sigma = pq(\mu_n + \mu_{p)}) \tag{3.40}$$

$$= (N_c N_v)^{1/2} q(\mu_n + \mu_p) e^{-E_G / 2k_B T} \tag{3.41}$$

This can be written as,

$$\sigma = A_0 e^{-E_G / 2k_B T} \tag{3.42}$$

where $A_0 = (N_C N_V)^{\frac{1}{2}} q(\mu_n + \mu_p)$ hence resistivity, ρ can be expressed as

$$\rho = \frac{1}{\sigma} = \frac{1}{A_0} e^{E_G / k_B T} = B_0 e^{E_G / k_B T} \tag{3.43}$$

Where $$B_0 = \frac{1}{A_0} = \frac{1}{((N_c N_v)^{\frac{1}{2}} q(\mu_n + \mu_p))} \tag{3.44}$$

The final expression suggests that the resistivity will decrease with increase in temperature for a semi-conductor.

3.6.2 Sheet Resistivity of thin films

Sheet resistivity of the fabricated films was measured following the Van der Pauw model. In this model, for very thin films (thickness t<<probe spacing's), current rings instead of spheres are realized. Therefore the area A can be expressed as;

$$A = 2\pi xt \tag{3.45}$$

where x is the distance between tips.

$$R = \rho x / \mathrm{A} \tag{3.46}$$

$$R = \int_{s}^{2s} \frac{\rho dx}{2\pi tx} \tag{3.47}$$

$$R = \frac{\rho}{2\pi t} \ln 2 \tag{3.48}$$

and

$$\rho_s = \frac{2\pi tR}{\ln 2} \tag{3.49}$$

Consequently, for

$$R = \frac{V}{2I}, \tag{3.50}$$

The resistance of the thin film sheet is given by: -

$$R_s = \frac{\pi}{\ln 2} F(Q) \frac{V_{DC} + V_{BC}}{2I} \left[\Omega / M^2 \right] \tag{3.51}$$

where F and Q are the symmetry and correction factors respectively. For $V_{BC} \leq V_{DC}, Q = \frac{V_{DC}}{V_{BC}}$ and vice versa. F is a function of Q and is valid for Q less than 10. It is expressed in the form;

$$F = 1 - 0.34657\left(\frac{Q-1}{Q+1}\right)^2 - 0.09236\left(\frac{Q-1}{Q+1}\right)^4 \tag{3.52}$$

$(V_{DC} + V_{BC})/2I$ is the average resistance

Average resistance is obtained from the slope of the average resistance curves using linear regression with the regression section selected manually. The specific resistivity ρ can be determined from the thin film thickness and the sheet resistance in the form;

$$\rho = Rt10^{-1}\,\mu\Omega cm \tag{3.53}$$

where t, is the film thickness.

3.7 Theory of Device Operation

The PRAM device geometry consists of three layers, an aluminum layer, a chalcogenide glass layer and a silver layer all on top of a glass substrate. The first layer of the device is an inert Aluminum layer that acts as the anode. On top of the anode comes the chalcogenide glass layer or the so called "memory film". This is the portion of the device that varies between a high resistance and low resistance state. The final layer is an inactive layer of silver that acts as the cathode of the device. The device operates by varying its resistance between high and low state under low biasing voltages. When a forward bias voltage is applied to the electrodes the chalcogenide thin film crystallizes and forms small conducting pathways between both electrodes. This is the low resistance state. Placing a reverse bias on the electrodes transforms the conduction pathways into amorphous state returning the chalcogenide thin film back to a high resistance state. The resistance state of the device determines the information stored either as a 1 or 0.

The next chapter presents a brief overview of the materials used in this research, the procedures adopted, and the precautions taken to ensure quality and desired results.

CHAPTER FOUR

MATERIALS AND METHODS

4.1 Introduction

This chapter presents a summary of the materials and methods used in the execution of this project in order to attain the objectives stated earlier. The research involved synthesis of Indium and Selenium alloys in varying ratios based on their molar masses, preparation of thin films from the samples, determining the film thickness, carrying out optical and electrical characterization and fabrication and testing of a prototype memory cell.

4.2 Synthesis of Indium and Selenium

Indium is silvery lustrous metal with a molecular mass of 114.818g and a melting point of 156°C. It has a reported electrical resistivity of $8x10^{-8}$ Ωm. Selenium on the other hand is a grey non metallic element with a metallic luster. It has a molecular mass of 78.96g and a melting point of 221°C. The electrical resistivity is $>10^{-8}$Ωm. Measured masses of Indium granules and Selenium pellets were mixed giving samples of ratios indium to selenium: 1:1, 1:2, 1:3, 2:3, 2:1, 3:1 by molar masses. These samples were afterwards each heated beyond their melting points (above 400°C) in oxygen free silica tubes to form alloys. Nitrogen being denser than oxygen was used to drive out air from the tubes before they were sealed and heated. The heating was done severally to ensure homogeneous mixing of the two materials. After cooling, the glass tubes were broken and the samples stored in air free plastic bottles. This was to prevent any possibility of an oxide forming.

4.3 In_xSe_y Thin Film Preparation

This was done using the Edwards AUTO 306 Vacuum coater. For each sample, five microscope slides were used. They first had their ends strip masked using aluminium foils fastened with kapton tape. This left the central portion of the slide unmasked where the film formed. The masking helped simplify the process of thin film thickness determination. The slides were then mounted on the substrate holder in the evaporation chamber of vacuum coater. Small portions of each sample were put in a molybdenum evaporator boat in the evaporation chamber of the Edwards AUTO 306 Vacuum coater and the chamber sealed. The chamber pressure was then pumped down to about $3x10^{-5}$mbar using the Turbo pumps connected to the Edwards AUTO 306 Vacuum coater. The power turned on and the current increased slowly up to 4A. In about five minutes all the material was found to have evaporated and formed a film on the slides. The power was switched off and the chamber allowed cooling. After attaining room temperature the chamber was vented and the slides removed, marked and packaged into a cardboard micro strip slide holder. The cardboard was then kept at temperatures below 20^oC. This was to avoid elevated temperatures, which would otherwise trigger oxidation.

4.4 Thin Film Thickness Measurement

This was done using Alpha IQ Surface Profiler. For thin film sheet resistivity calculation, film thickness is an important parameter. Many techniques exist for thin film thickness measurement and include; ellipsometry, interferometry, quartz crystal oscillators and stylus-method profilometry and others (Ohring, 2002). In this study, the latter technique was used. The method involves measuring the mechanical movement of a

diamond needle (stylus) as it is made to trace the topography of the film- substrate step. The steps were introduced during the films preparation by masking parts of the substrates with aluminium foil before deposition. To measure thickness, thin films were placed on the profilometer device stage and then fine stylus dragged across the film surface. When the stylus encountered steps, signal variations (based on a differential capacitance or inductance technique) indicated the step heights. This information was then displayed on a computer screen as film thickness.

4.5 Optical Characterization of the Films.

The objective of optical characterization was to determine the optical properties of the films, which include; reflectance, transmittance, absorption coefficient, refractive index and dielectric function. Spectral reflectance and transmittance of the thin films were measured using the Solid Spec 3700 spectrophotometer machine. The process involved probing first a plain microscope slide with a radiation of known wavelength and frequency to establish its reflective and transitive property. Thereafter a similar slide with a film is probed. The difference in the values is a measure of the reflectance and transmittance of the film alone respectively. The figure 4.1 below was the set up during optical characterization.

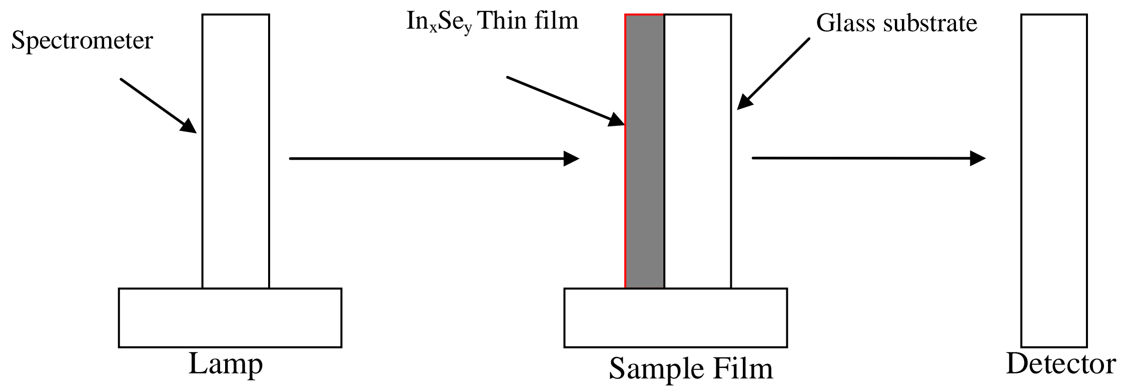

Figure 4.1: Schematic diagram showing optical transmission measurements.

After obtaining raw data for both reflectance and transmittance, the Scout software by Wolfgang Theiss was used to obtain simulated data from the measured data. The simulated data was used to deduce the optical constants of the films.

4.5.1 Optical band gap of the films

To obtain the optical band gap (E_g), of the films, graphical method was used. Figure 4.2 shows a spectral plot of the square of the product of absorption coefficient, Planck's constant, and the frequency of the probing radiation $(\alpha h\upsilon)^2$ against photon energy which is used to establish the type of band gap and also by extrapolating the near straight part of the graph to the energy axis, the value of the band gap energy was determined. The value of the x intercept, $(\alpha h\upsilon)^2 = 0$, corresponds to the band gap energy.

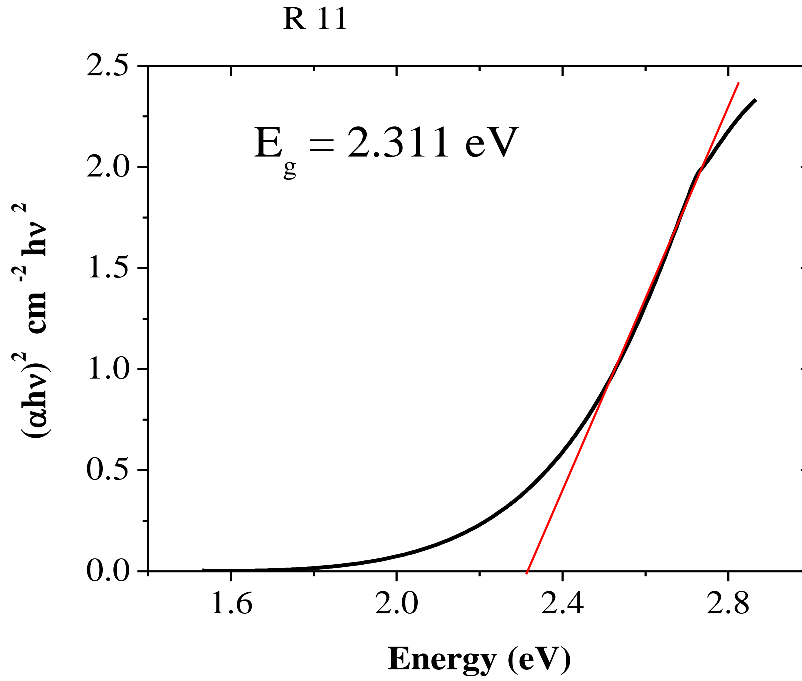

Figure 4.2: Plot of the square of the product of absorption coefficient, Planck's constant and frequency, $(\alpha h\upsilon)^2$ against photon energy

Absorbance has an exponential decay with increase in wavelength. This is because the photon energy is less than the band gap hence excitation of electron in valence band to cross to the conduction band. Absorption coefficient (α) is related to photon energy ($h\upsilon$) by the following relation:

$$\alpha = \frac{(h\nu - Eg)^{1/2}}{h\nu} \tag{4.1}$$

Hence

$$(\alpha h\upsilon)^2 = h\upsilon - E_g \tag{4.2}$$

Where h is Planck's constant (6.62×10^{-34}Js) and υ the frequency of the incident photon (Eya et al, 2005). By plotting $(\alpha h\upsilon)^2$ against $h\upsilon$, band gap of a film can be obtained at $(\alpha h\upsilon)^2 = 0$ (Ndukwe, 1998 and Ndukwe, 1996).

4.6 Electrical Characterization.

The electrical resistance and sheet resistivity of the thin films were measured using the four point probe system assembled by Agumba 2010 in line with the Van der Pauw approach.

4.6.1 The Four Point Probe Technique

The four point probe technique was used to measure the sheet resistivity of the In_xSe_y semiconductor thin film samples. A symmetrical square geometry was adopted where the four leads from the designed probe head were connected to Keithley Sourcemeter via the switching device as per the Van der Pauw set-up for Voltage and Current measurements. The schematic diagram of four-point probe resistivity measurement is as shown in figure 4.3 below. A current of 1.0×10^{-10} A was applied through the contacts A and B and the potential drop V_{DC} across the contacts D and C measured. With switching of probe tips on the sample done by the developed switching device, the same amount of current (I) was then applied

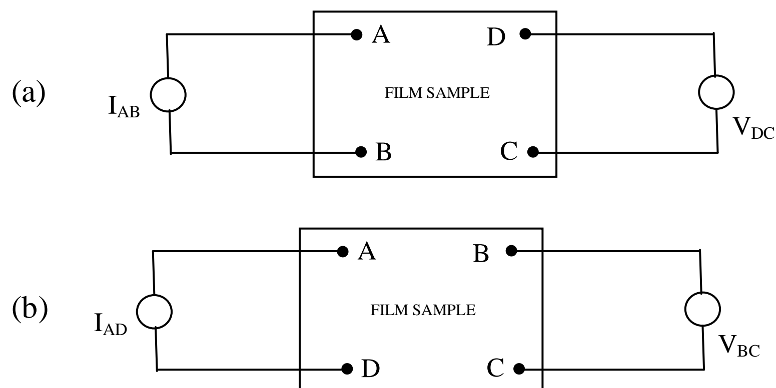

Figure 4.3(a) and (b): Schematic diagram of four-point probe resistivity measurement using the Van der Pauw method (Agumba, 2010).

Through the contacts A and D and the potential drop V_{BC} across the contacts B and C measured. These values of current, measured voltage drops and film thickness were used to compute sheet resistivity by the developed LabVIEW software. The sheet resistivity measurements of the film samples were first performed at room temperature (24°C). Thereafter the resistivity of the film samples was measured at varying temperatures by placing the samples in a Lindberg/Blue Tube FurnaceTF55035A model.

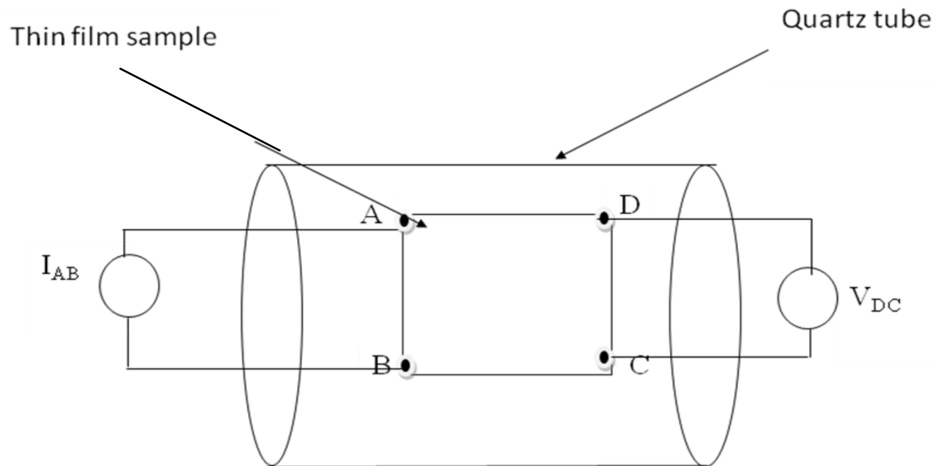

Figure 4.4: Schematic representation of set up used during sheet resistivity measurements at different temperatures.

4.7 Device Fabrication

Figure 4.5 is a cross-section of the memory device fabricated. The three thin film layers are deposited from the same thermal evaporator in three sessions. In between each session, the device slides are stored in nitrogen ambient.

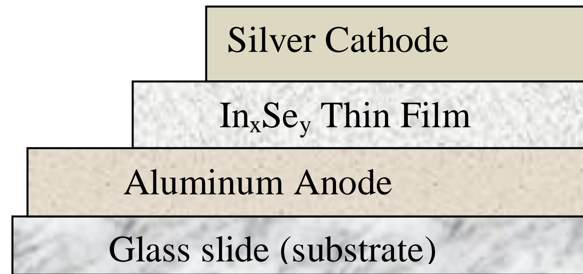

Figure 4.5: Schematic diagram of vertical cross- section of PRAM test device

After optimization of the film samples, four slides were used to prepare thin films of In_xSe_y with a ratio of 1:3 for device testing. This sample had a higher band gap suitable for formation of electron hole pairs, low sheet resistivity thus reducing the power consumption, and low crystallization temperature for faster switching. The four slides were cleaned with ethanol and then left out for drying before being blown clean using nitrogen.

4.7.1 Aluminum Anode back contact layer

The first layer on the slide is the aluminum anode. The molybdenum boat was filled with granules of aluminum. Thereafter, the slides were fixed securely on the slide holder using kapton tape. The evaporation chamber pressure was then pumped down to about $3x10^{-5}$ torr. A current of about 4A was passed through the boat for about 1 minute which caused melting and evaporation of the aluminum on the slides. The chamber was vented using the atmosphere, the slides removed and stored in nitrogen ambient. The procedure was repeated for layers two and three with respective materials.

4.7.2. $InSe_3$ Thin Film layer

The evaporation boat was cleaned with ethanol, dried and blown with nitrogen. It was then replaced in its position between the two electrodes of the heating circuit. The slides with aluminum anode were masked a third way each from one end using kapton tape and fixed securely on the substrate holder as shown in figure 4.6. A small lump of $InSe_3$ was put in the molybdenum boat, the evaporation chamber was sealed and the pressure pumped down to about $3x10^{-5}$ mbar. A current of about 4A was passed through the heater circuit for about two minutes and all the compound was found to have evaporated onto the aluminum layer.

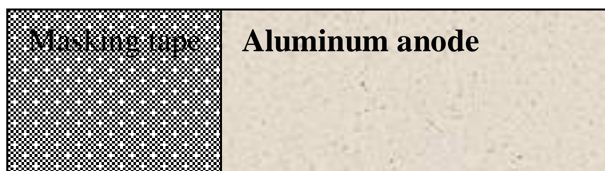

Figure 4.6: Illustration of the masking of one side of slide before the layer of In_xSe_y is added.

4.7.3 Silver Cathode top electrode

After the layer of $InSe_3$ had been added the chamber is vented as before, the slides kept in nitrogen ambient as the chamber was made ready for adding the silver cathode layer. The boat was cleaned with ethanol, dried and blown clean using nitrogen. The silver cathode layer a thin coating of silver paint which overlaps with the chalcogenide layer and not having any contact with the aluminum anode as shown in figure 4.7.

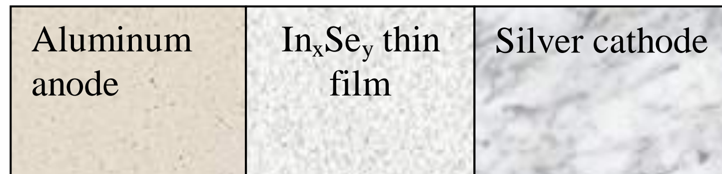

Figure 4.7: Schematic illustration of the aerial view of the Phase Change Memory (PRAM) test device

4.8 PRAM test device testing

Using Keithley 2400 source meter the device was tested. The slide was secure with clips at the extreme ends as terminals then a voltage applied, and the current drawn recorded after stabilizing. The voltage applied started from zero and increased until 1.5 volts and then decreased until -1.5 volts, then back to zero volts. The process took about 10 minutes.

CHAPTER FIVE

RESULTS AND DISCUSSION

5.1 Introduction

This chapter presents results of the optical and electrical properties of the In_xSe_y thin film samples prepared at different concentrations by molar mass. From the material properties, the sample with optimal features was used to fabricate a PRAM test device, which was characterized to determine its operational suitability.

5.2 Optical Characterization of the films

5.2.1 Optical properties

5.2.1.1 Transmittance, Reflectance and Absorbance

Figures 5.1 and 5.2 represent spectral plots of experimental data for reflectance and transmittance against the wavelength of the probing radiation. The spectral graphs of reflectance against wavelength revealed that within the visible range the films exhibited minimal reflection, at almost less than 50% for all film samples, with the exception of the film sample with the ratio of 1:1. Beyond the visible region, there is a marked increase in reflectance mostly for the film with the ratio of 2:1, which goes above 50%. This is attributable to reduction in photon energy of the incident radiation. Films having a high concentration of selenium exhibited interband transitions as evidenced by the sharp peaks. Here, the electrons from the filled states at the top of the valence band absorb

incident photon energy almost equal to energy band gap and hence photo- exited to the empty states in the conduction band. These peaks are attained within energy range, which corresponds with the energy band gaps of the films. The sharp peaks occur at the fundamental absorption or transition.

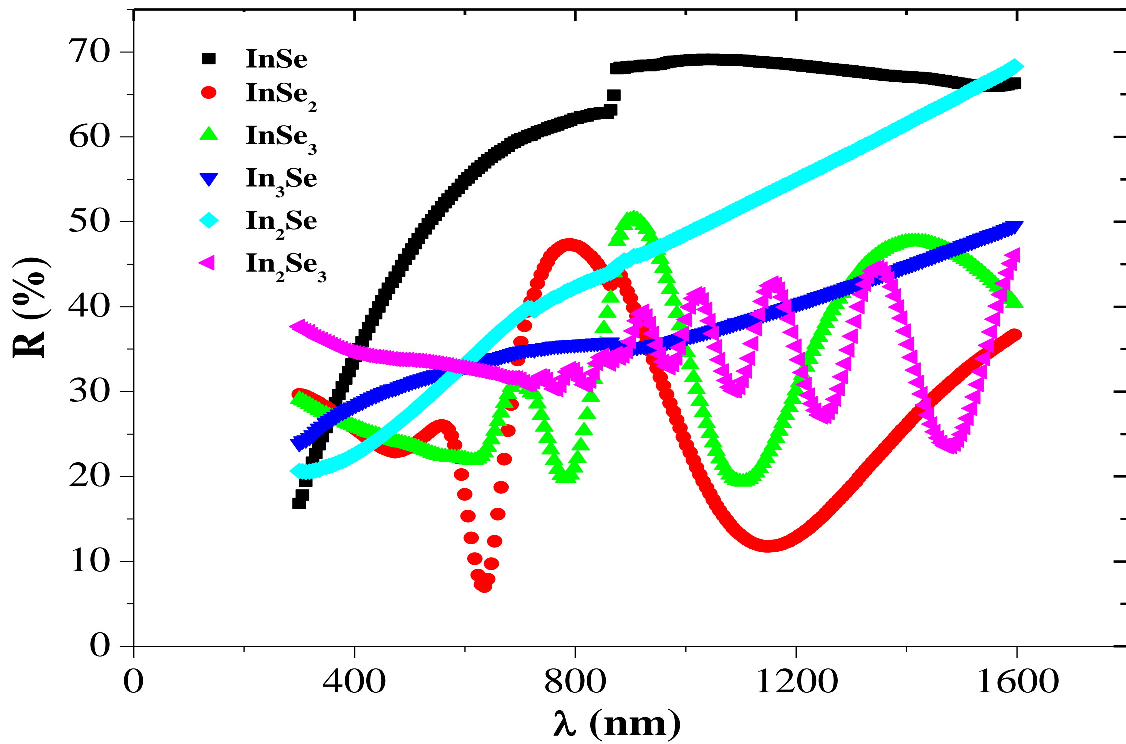

Figure 5.1: Spectral graph of percentage reflectance against wavelength (nm) for the as deposited thin films of indium and selenium.

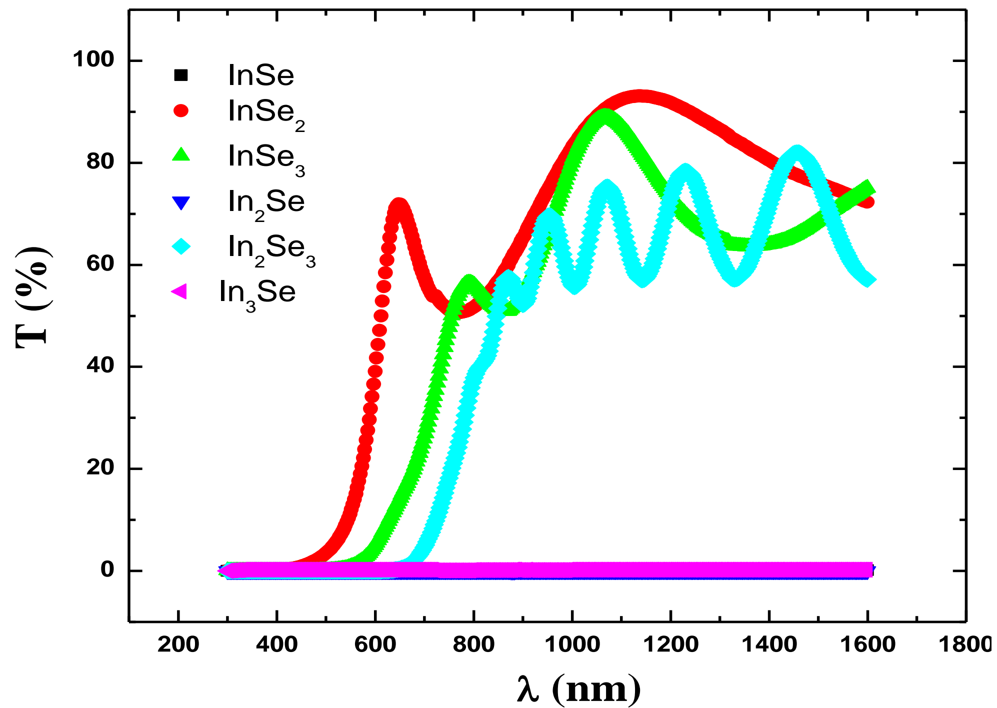

Figure 5.2: Spectral graph of percentage transmittance against wavelength (nm) for the as deposited thin films of indium and selenium.

A survey of the transmittance spectra for the films reveals that films with a high concentration of selenium have an average transmittance of over 50% within and above the visible range. These films exhibit interference at higher wavelengths. On the other hand, films with equal or higher concentration of indium to selenium have negligible transmission. These films either absorb or reflect the energy of the radiation.

The transmittance, reflectance and absorbance data obtained were used to obtain simulated data that was used to determine the optical constants. Using the Scout software by Wolfgang Theiss (2000) and the OJL model together with harmonic oscillator susceptibility, optical constants for the films were obtained. Figure 5.3 shows spectral

fitting of experimental and simulated data for purposes of obtaining optical constants for a film with Indium to Selenium ratio of 3:1

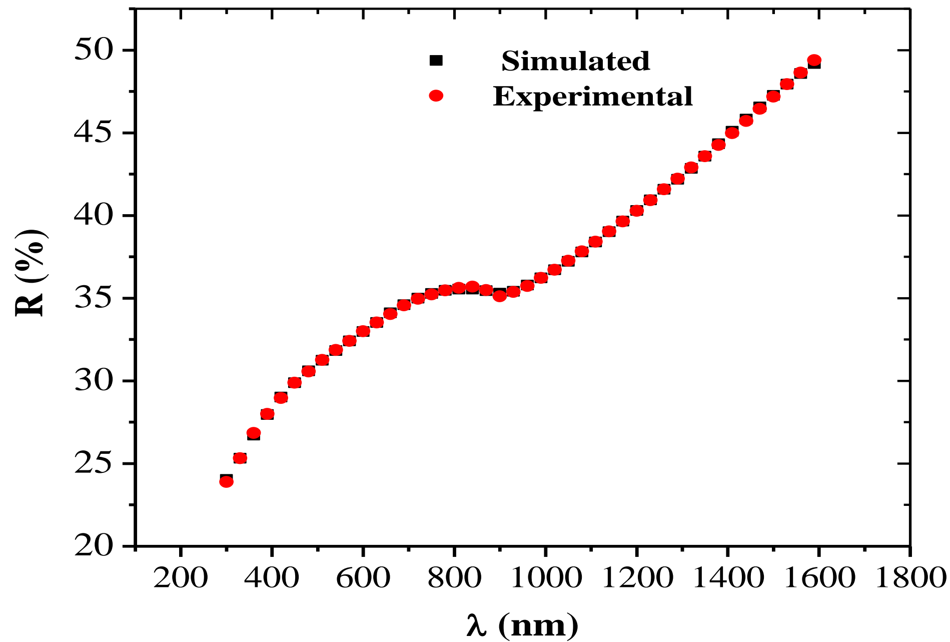

Figure 5.3: A graph showing a sample fitting of percentage reflectance against wavelength (nm) of experimental data to obtain simulated data for a In_3Se film.

As seen from the spectral plot, there is great agreement between the measured data and simulated data within the visible region (300-790nm). The optical constants including the refractive index and absorption coefficient were extracted from the simulations.

5.2.1.2 Energy band gaps of In_xSe_y films

The simulations obtained after fitting the experimental data using the Scout software were used to establish optical properties of the films like the absorption coefficient, the refractive index and the band gap energies.

The band gap energies of the semiconductor thin films were determined using the relation given by Ndukwe (1998) below;

$$(\alpha h\nu)^2 = h\nu - E_g \tag{5.1}$$

By extrapolating the linear portions of the plots of $(\alpha h\nu)^2$ against $h\nu$ to where $(\alpha h\nu)^2 = 0$, the value where the line cuts the energy axis is the band gap value (Palik, 1985).

Figure 5.4 shows how the band gap values of the films were obtained.

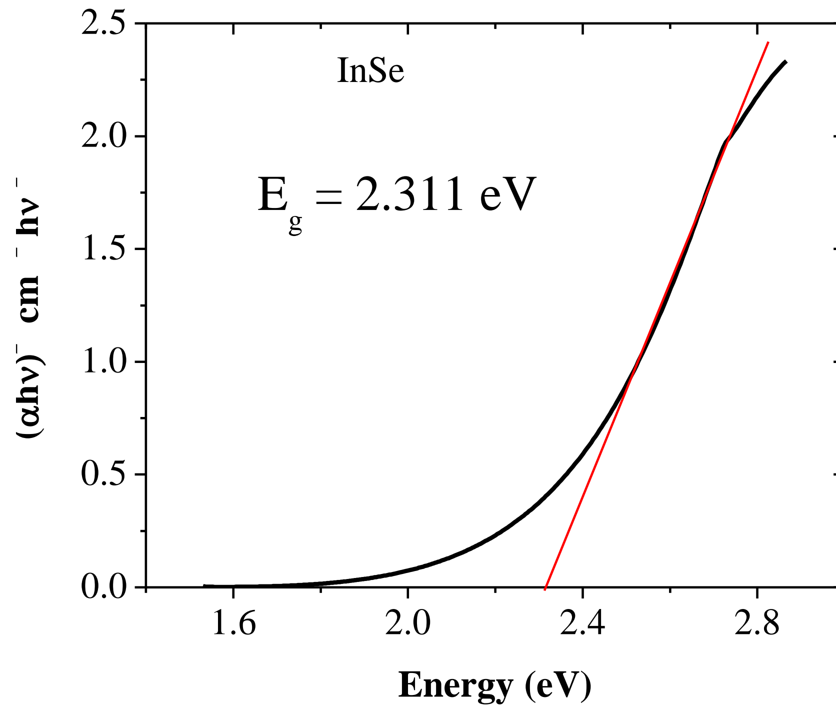

Figure 5.4: Graphical determination of band gap of InSe thin film.

Table 5.1: Summary of the band gap energies of the films under investigation

Sample (In/ Se) Concentration	Energy Gap (eV)
1:3	2.67
1:2	2.41
2:3	2.35
1:1	2.31
2:1	2.18
3:1	2.07

The corresponding graphical representation of the variation of band gap with In/Se concentration is shown in Figure 5.5.

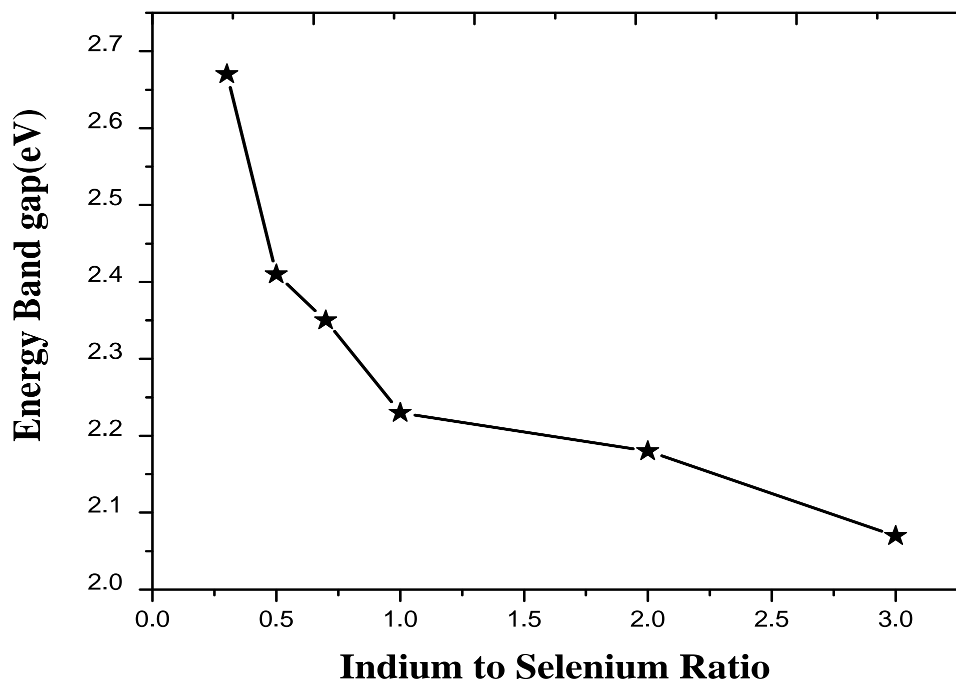

Figure 5.5: Graphical variation of band gap energy (eV) with Indium to Selenium concentration in the films.

From figure 5.5, it can be seen that the band gap of the films increased with increasing selenium concentration in the films. These results agree closely with those of Gopal *et al.* (2005), who noted an increase in band gap with increasing selenium content in the film samples. However, the films were prepared from a chemical route in a chloride ambient.

5.2.1.3 Refractive index of the film samples

Values of the refractive indices were plotted against photon energies and the graphs in figure 5.6 obtained.

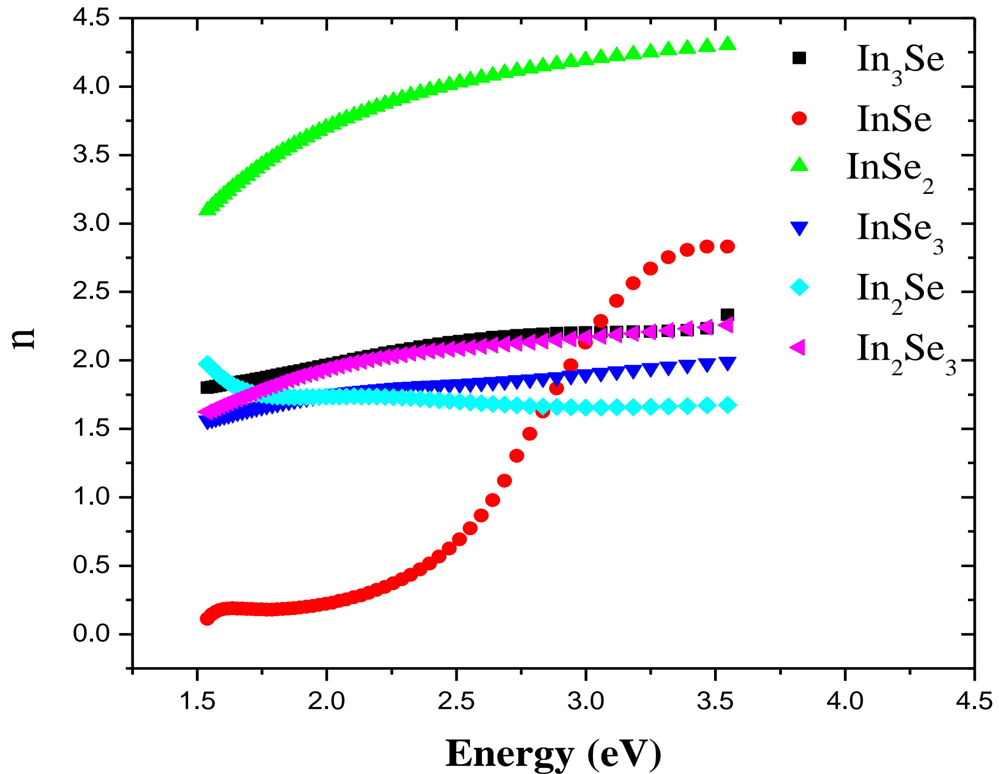

Figure 5.6: Spectral Graphs of refractive index against photon energy for the as deposited film samples of Indium and Selenium.

5.3 Electrical properties of the thin films

The films fabricated were characterized where the sheet resistivity of each of the samples was determined using the four point system assembled by Agumba 2010. First, the sheet resistivity of the films at room temperature was investigated. Thereafter, the sheet resistivity during annealing was performed.

The procedure at room temperature was a simple one where the designed system was interfaced to a computer with a labVIEW running program. The current and voltage values were sourced from the Keithley source meter and using the software values of the sheet resistivity for the film samples was computed. Table 5.2 gives the results obtained.

Table5.2: Indium/ Selenium ratio and the sheet resistivity at room temperature.

Indium to selenium ratio	Sheet resistivity (x 10^2 Ωcm)
3:1	1.09602
2:1	1.08159
2:3	1.05945
1:1	1.04945
1:2	1.04861
1:3	1.02849

A graphical comparison of how the resistivity varies with concentration is as shown in figure 5.7.

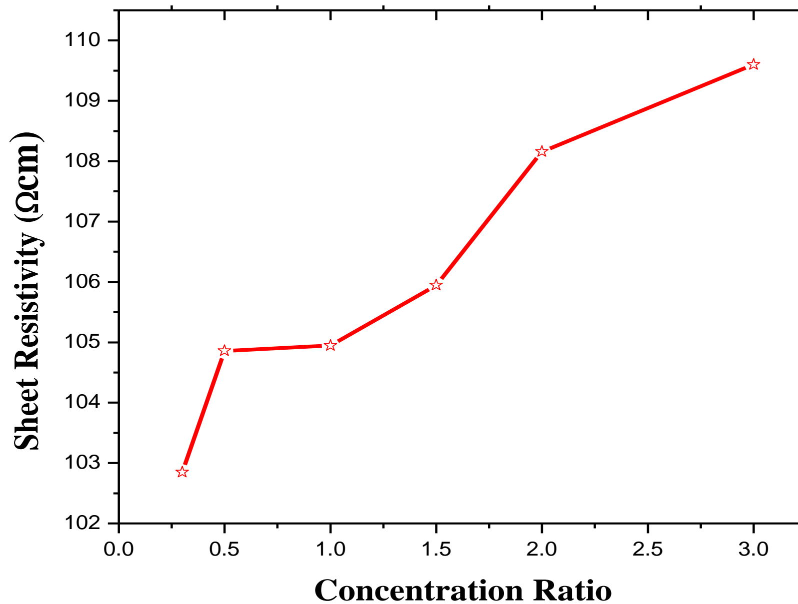

Figure 5.7: Graphical variation of Sheet resistivity (Ωcm) with Indium to Selenium concentration in the film samples.

It is apparent from figure 5.7 that an increase in indium in the film resulted in increased sheet resistivity of the film. These results can be attributed to variations in the strengths of the bonds formed during synthesis of the samples and film deposition.

During annealing, the films were put in a specially designed tube fitted into the furnace. Argon gas was passed through the tube (to eliminate air, which may cause oxidation of the films during heating) before being sealed. The furnace was set for the temperatures ranging from room temperature to about 450°C at the rate of 5K/Min. The results obtained were used to plot the graph in figure 5.8 which clearly indicates the phase change behavior of the alloy. As the temperature increases, there is a decrease in the sheet resistivity of the films.

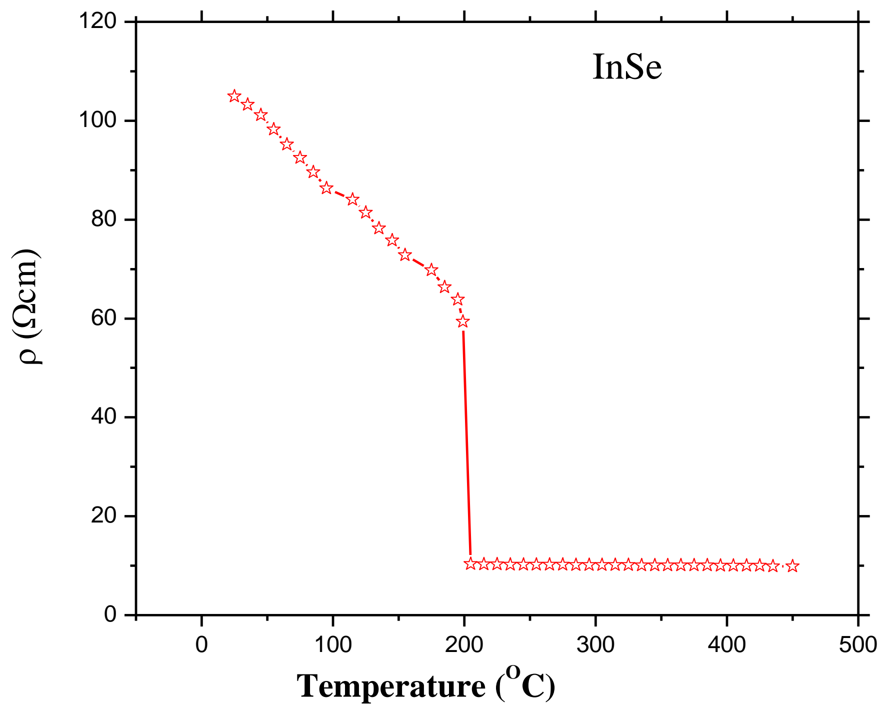

Figure 5.8: Graphical variation of sheet resistivity against temperature during thermal cycling.

The graph of the derivative of the sheet resistivity against temperature gives the crystallization temperature at the lowest point of the graph. Figure 5.9 below shows how the crystallization temperatures of the films were obtained.

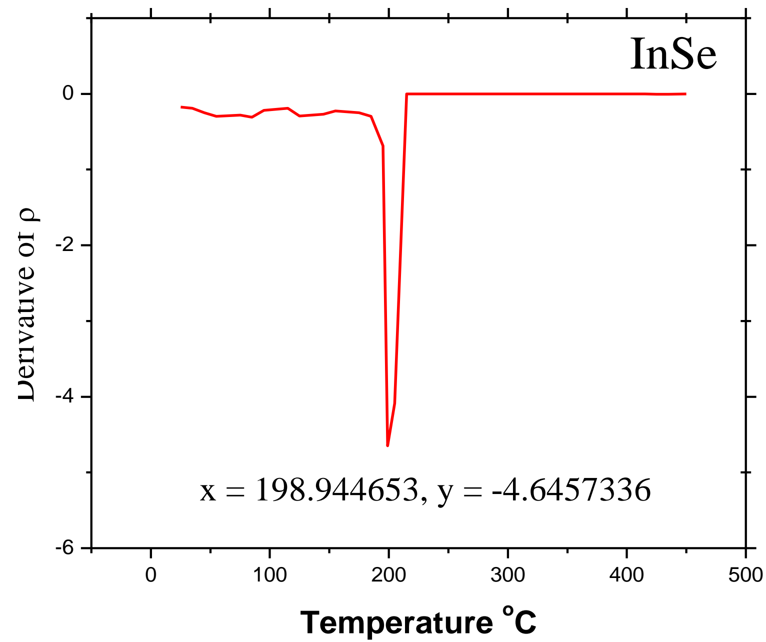

Figure 5.9: Derivative of sheet resistivity (Ωcm) against temperature for the film with indium to selenium ratio of 1:1

Table 5.3 gives a summary of the results for the band gap energies of the thin films, their crystallization temperature and sheet resistivities.

Table 5.3: Summary of the variation of the crystallization temperature with Indium/Selenium ratio

In/Se concentration	**Band gap (eV)**	**Sheet resistivity at room temp. ±0.5**	**Crystallization Temp (^{o}C) ±0.5**
1:3	2.67	102.85	194.56
1:2	2.41	104.86	196.75
2:3	2.35	105.95	199.98
1:1	2.26	104.95	198.94
2:1	2.18	108.16	201.14
3:1	2.07	109.60	203.33

From table 5.3 above, it can be seen that film with Indium to Selenium ratio of 1:3 has the lowest sheet resistivity, lowest crystallization temperature and highest band gap. The lower sheet resistivity ensures low power consumption since phase change is a thermally driven process. Also the low crystallization temperature ensures faster switching while at the same time the high band gap energy rules out the possibility of the standby conditions influencing electrical conductivity. From this, a memory cell was fabricated and a static mode test done using the Keithley 2400. The graph in figure 5.10 below shows the I-V characteristics during SET and RESET operations.

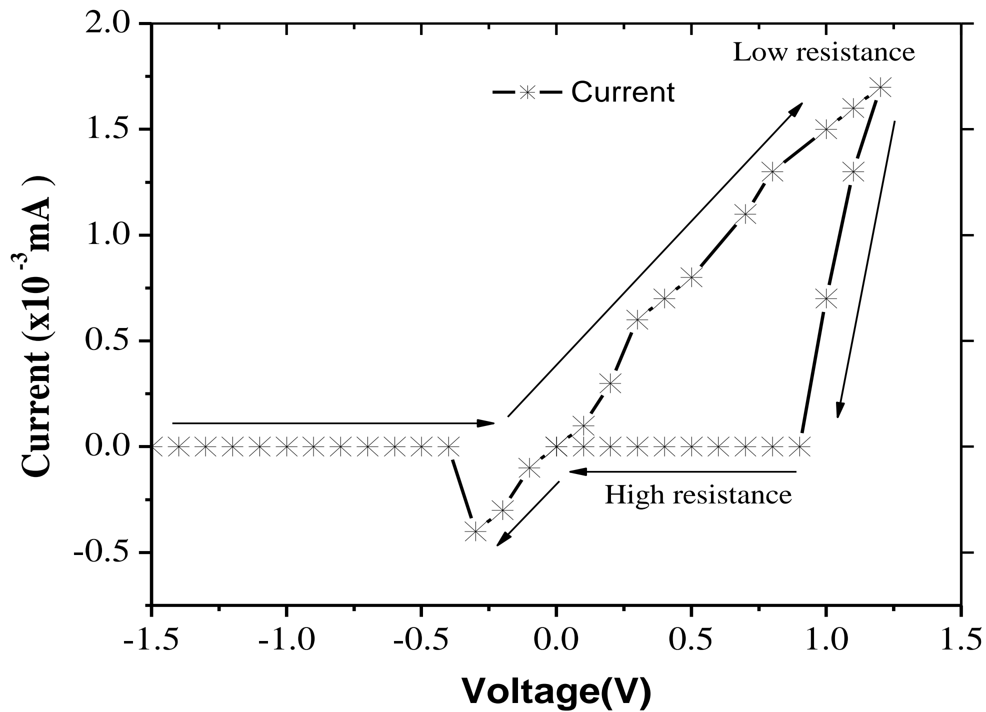

Figure 5.10: Static mode I-V characteristics of $InSe_3$ PRAM test device.

From the graph in figure 5.10, it can be seen that the memory device can be turned to a low resistive state and a high resistive state just as theory predicts. The device switches from a low resistive state upon application of 0.9V bias, while it can be turned to a high resistive state upon application of -0.4V reverse bias. The resistance difference between the on state and the off state is significant enough to be sensed using current sensors.

Out of the six devices fabricated only two seemed to switch between high and low resistances. The reason attributable to this could be that the other four devices were shorted, open or questionable (Dunn, 2008).

CHAPTER SIX

CONCLUSION AND RECOMMENDATIONS

6.1 Conclusion

The main objective of this study was to investigate the relationship between the concentration of indium and selenium in the phase change material and its sheet resistivity at room temperature and during annealing. This was made possible first synthesizing Indium and Selenium into various compositions by mass and evaporating thin films of the samples on glass substrates by single source evaporation. This was done using the Edwards auto 306 Magnetron sputtering system where samples were placed on a molybdenum boat and the chamber pressure pumped down to about $3.5x10^{-5}$ mbar before commencing heating with a current of 4A. This was done within a period of two minutes.

Optical spectroscopy was performed on the various film compositions to determine the bandgap energy and other optical parameters including the refractive index and film thickness. The optical data obtained from the spectrophotometer showed great dependence of the optical properties on the concentration of indium and selenium in the film. Films with high concentration of indium for instance were more reflective beyond the visible region whereas those with a greater concentration of selenium were more transitive above the visible region and zero transmittance with low selenium. The optical band gap energy of the films increased with increase in selenium content up to 2.67eV. The film thickness ranged from 80 nm to 120 nm.

The sheet resistivities of the various thin film samples at room temperature and during annealing were determined. The as deposited films (amorphous) had a sheet resistivity which depended on the ratio of indium to selenium. The film having the highest concentration of indium had the highest sheet resistivity (109.6Ωcm). This observation agrees with that of Gopal *et al.* (2005) who investigated the influence of the ratios from a chemical route. The crystallization temperature again heavily depended on the ratio of Indium to Selenium in the film. It was noted that the film sample with the ratio of Indium to Selenium 3:1 had the highest crystallization temperature of 203.3^{o}C. The PRAM test device was fabricated and its I-V characteristics studied. The PRAM test devices fabricated had the on voltage of 0.9V and off voltage of -0.4V with peak write current of 1.7×10^{-3}mA and peak erase current of -4×10^{-4} mA.

6.2 Recommendations

Before chalcogenide based devices can be put to commercial use there are still several issues that require further study. These issues include the fabrication of chalcogenide films with higher homogeneity, integration of chalcogenide devices with silicon devices, the effects if any of oxidation layers between electrodes and the chalcogenide glass thin films, scalability of devices and a functional mathematical model of the working of chalcogenide devices. The quality of the films can greatly be improved by carrying out measurements in situ. Molecular beam epitaxy (MBE) for instance, is more advantageous than single source evaporation used in this study. It involves controlled evaporation in an ultra high vacuum ($\sim10^{-10}$ torr) system. Interaction of one or more evaporated beams of atoms or molecules with the single crystal substrate yields the desired epitaxial film. The clean environment coupled with the slow growth rate and independent control of the

beam sources enables the fabrication of semi-conductor heterostructures at an atomic level. However, equipments that can assist in doing this are quite expensive.

Another method of film growth would have been by electron beam evaporation. The disadvantages of resistively heated evaporation sources include possible contamination by crucible heaters and support materials and the limitation of relatively low input power levels. This makes it difficult to deposit pure films or evaporate high melting point materials at appreciable rates. Electron beam heating eliminates these disadvantages. In principle this type of source enables evaporation of virtually all materials at almost any rate. The purity of the evaporant is ensured because only a small amount of charge melts or sublimes so that the crucible is the connected skull material next to the cooled hearth. For this reason there is no contamination of the evaporant by copper. Multiple source units are available for sequential or parallel deposition of more than one material.

Rutherford's Backscattering Spectroscopy (RBS) and X-ray photoelectron spectroscopy should be performed on the thin films to analyze their compositional stoichiometry and structural effects. Further, X-ray diffraction (XRD) could be performed on the films to ascertain the crystallinity of the films.

REFERENCES

Agumba, J. O. (2010). Design and fabrication of a simple four point probe system for electrical characterization of thin films. MSc Thesis. Kenyatta University.

Almen, O. and Bruce, G. (1961). Collection and Sputtering experiments with noble gas ions. *Nuclear Instruments and Methods,* **11**(1): 257-278.

Anderson, J. C. Leaver, K. D. Rawlings, R. D. Alexander, J. M (1985). Material`s Science, Third Edition. The Thetford Press Ltd, Thetford, Norfolk. Great Britain. Pp 419-421.

Bautista, K. (2004). Thin film deposition, 2nd edition, University of Texas at Dallas, Erik Jonsson School of Engineering, USA.

Blood, P. Orton, J.W (1996). The Electrical Characterization of Semiconductors: Majority Carriers and Electron States, Academic Press Ltd, London. Pp 26-53.

Bo L., Zhitang S., Songlin F., Bomy C. (2005). Characteristics of chalcogenide non volatile memory nano-cell-element based on Sb2Te3 material. *Microelectronic Engineering*, **82**:168-174.

Brown,M. & Jakeman, (1996). Theory of four point probe technique as applied to film layers on conducting substrates, *British Journal of applied Physics*, **17:**1146-1149.

Burr G. W., Breitwisch M. J., Franceschini M., Garetto D., Gopalakrishnan K., Jackson B., Kurdi B., Lam C., Lastras L.A., PadillaA., Rajendran B., Raoux S., and Shenoy R. S.(2010). Phase change Memory Technology. *Journal of Vacuum Science and Technology,* **28**(2): 223-262.

Cheng K. (2001). Evaluation of Crystallization Kinetics of Glasses by Non- isothermal Analysis. *Journal of Material Science*. **36**: 1043-1048.

Coombs J. H., Jongenelis A. P. J. M., Vanesspiekman W. and Jacobs B. A. J. (1995). Laser-induced crystallization phenomena in GeTe based alloys and composition dependence of nucleation and growth. *Journal of Applied Physics,* **78**(8):4918-4928.

Dunn W. P. (2008). Fabrication and Testing of a Non Volatile Memory using a chalcogenide glass film. MSc Thesis, California Polytechnic State University.

Eya, D., Ekpunobi, A., Okeke, C. (2005). Optical properties of cuprous oxide thin films prepared by chemical bath deposition technique. *The Pacific Journal of Science and Technology,* **6**(2): 98-104.

Gopal S., Viswanathan C., Karunagaran B., Narayandass K. S., Mangalaraj D. and Junsin Y.(2005). Preparation and characterization of electrodeposited indium Selenide thin films. *Journal of Crystallization Research Technology,* **40**(6): 557-562.

Greene, Kate "A Memory Breakthrough," Technology Review, 04-Feb-2008

Grovenor, C. R M. (1989). Microelectronic Materials, Institute of Physics Publishing, Bristol and Philadelphia. Pp71-184.

Heireche L. and Belhadji M. (2007). Non-isothermal Crystallization in $Ge_{15.4-x}Te_{84.5}Sb_x$ ($0.5<x<1.5$) *Journal of Ovonic Research,* **3**: 15-20.

Heon, Lee. Kim, K.Y. (2005). Indium Selenide (In_2Se_3) thin film for phase-change memory.

Heon, Lee. Kim, K.Y. (2005). Switching Behavior of Indium Selenide-Based Phase Change Memory Cell.

http://www.technologyreview.com/Biztech/20492/? a=f 24.08.08.

http://www.technologyreview.com/Infotech/20148/? a=f 24.08.08.

Hwang, Y.N.(2003). "Full integration and reliability evaluation of phase change RAM based on 0.24μm-CMOS technologies," in VLSI Symp.Tech. Dig., p l73.

Kalb J., Spaepen F., and Wuttig M., (2004). Atomic force microscopy measurements of crystal nucleation and growth rates in thin films of amorphous Te alloys. *Applied Physics Letters,* **84**(25):5240-5242.

Kolobov A.V., Fons P., Tominaga J., Frenkel A.I., Ankudinov A.L., Yannopoulos S.N., Andrikopoulos K.S. and Uruga T. (2005). Why Phase Change Media Are Fast andStable: A New Approach to an Old Problem. *Japanese Journal of Applied Physics,* **44**: 33245-3349.

Kristy, A., Christopher, M. (2007). Phase change memory devices with stacked Ge-chalcogenide/Sn- chalcogenide layers. *Microelectronics Journal*, **38**: 52-59.

Lai S. (2003). Current status of the phase change memory and its future. *In IEDM Technical Digest* pages 10.1.1-10.1.4

Lankhorst M.H.R., Ketelaars B.W.S.M.M. and Wolters R.A.M. (2005). Low cost and nanoscale non-volatile memory concept for future silicon chips. *Nature Materials* **4**(4):347-352.

Lee J., Ni H. and Ramirez G.A. (2005). Compositional effects on the crystallization kinetics of NiTi thin films. *Journal of Material Resources,* **20**(7):1728-1734.

Masuoka, F.(1996) “Flash Memory Technology,”Proc. Int. Electron Devices Mater. Symp., 83,Hsinchu, Taiwan.

Matsuzaki N., Kuotsuchi K., Matsui Y., Tonomura O., Yamamoto N., Fujisaki Y., Kitai N., Takemura R., Osada K., Hanzawa S., Moriya H., Iwasaki T., Kawahara T., Takaura N., Terao M., Matsuoka M. and Moniwa M. (2005). Oxygen doped GeSbTe phase change memory cells featuring 1.5V/100-standard 0.13m CMOS operations. *In IEDM Technical Digest.* Pp 738-741.

Mehta N., Zulfequar M. and Kumar A. (2004). Crystallization kinetics of some Se - Te - Ag chalcogenide glasses. *Journal of Optoelectronics and Advanced Materials,* **6**: 441-448.

Ndukwe, C. (1996). Solar energy materials and solar cells. **40**(123)

Ndukwe, C. (1998). *Nigerian Journal of Physics*, 10:7.

Njoroge W.K. and Wuttig M. (2001). Crystallization kinetics of sputter deposited amorphous AgInSbTe films. *Journal of Applied Physics* **90**(8):3816-3821.

Ohring, M. (1992). The material Science of thin films, Academic Press, United Kingdom.
Ohshima N. (1996). Crystallization of Germanium-antimony-tellurium amorphous thin films sandwiched between various dielectric protective films. *Journal of Applied Physics,* **79**(11):8357-8363.

Ovshinsky S.R. (1968). Reversible electrical switching phenomena in disordered structures. *Physical Review Letters,* **21**(20):1450.

Owade, M. (1998). Design and Development of a programmable interface system with illustrative use in resistivity-temperature experiment, MSc. Thesis, Kenyatta University.

Panish, M. B and Temkin, H. (1989*). Annual Review of Material Science.* **19**(209).

Park J.B., Park G.S., Baik H.S., Lee J.H., Jeong H. and Kim K. (2007). Phase change behavior of stoichiometric $Ge_2Sb_2Te_5$ in phase change random access memory. *Journal of Electrochemical Society,* **154**(3):H139-H141.

Park S.J., Kim I.S., Kim S.K., Yoon S.M., Yu B.G. and Choi S.Y. (2008). Phase transition characteristics and device performance of Si-doped $Ge_2Sb_2Te_5$. *Semiconductor Science and Technology,* **23**:105006 4pp.

Pellizzer, F. Lacaita, A. Redaelli, A. Lelmini, D. Pirovano, A. Benvenuti, A. (2004) *IEDM Technology Digest.*Pp 911.

Pirovano A., Lacaita A.L., Benvenuti A., Pellizzer F., Hudgens S. and Bez R. (2003). Scaling analysis of phase change memory technology. *In IEDM Technical Digest* **29**(6):1-4.

Pirovano A., Redaelli A., Pellizzer F., Ottogali F., Tosi M., Ielmini., Lacaita A.L. and Bez R. (2004). Reliability study of phase change nonvolatile memories. *IEEE Transactions on Device and Materials Reliability,* **4**(3):422-427.

Ploog, K. (1981). *Annual Review of Material Science,* **19:**171.

Qiao B., Yun L., Lin Y., Lai L., Feng J., Chen B. and Tang T. (2006). The performance of GeSbTe material for PCRAM device. *Integrated Ferroelectronics Journal,* **10**: 261-270.

Rao T.L., Dhurandhar H.D., Lad K.N. and Pratap A. (2008). Kinetic analysis of crystallization processes in amorphous 2826A ($Ni_{36}Fe_{32}Cr_{14}P_{12}B_6$) metallic glass. *Indian Journal of Pure and Applied Physics,* **46**: 390-393.

Raoux S. (2009). Phase change materials. *Annual Review of Material Research,* **39**: 25-48.

Raoux S., Cheng H., Munoz B. and Jordan-sweet J. (2009). Crystallization Characteristics of Ge-Sb and Ge-Te Phase change Materials. *Europe Phase Change Ovonic Science Symposium.* Pp 91-98.

Raoux S., Jordan-Sweet J.L. and Kellok A.J. (2008). Crystallization properties of ultra-thin phase change films. *Journal of Applied Physics,* **103**(11):114310.

Raoux S., Shelby R., Munoz B., Hitzbleck M., Krebs D., Salinga M., Woda M., Austgen M., Chung K. and Wuttig M. (2008). Crystallization Times of As deposited and Melt-quenched Amorphous Phase Change Materials. *Europe Phase Change Ovonic Science Symposium.* Pp 40-47.

Redaelli A., Ielmini D., Lacaita A.L., Pellizer F., Pirovano A. and Bez R. (2005). Impact of crystallization statistics on data retention for phase change memories. *In IEDM Technical Digest.* Pp 742-745.

Redaelli A., Ielmini D., Russo U. and Lacaita A.L. (2006). Intrinsic data retention in nanoscale phase change memories. Statistical analysis and prediction of failure time. *IEEE Transaction on Electron Device,* **53**(12):3040-3046.

Redaelli A., Pirovano A., Pellizer E., Lacaita A.L., Ielmini D. and Bez R. (2004). Electronic switching effect and phase change transition in chalcogenide materials. *IEEE Electron Device letters,* **25**(10):684-686.

Russo U., Ielmini D., Redaelli A. and Lacaita A.L. (2006). Intrinsic data retention in nanoscale phase change memories. Monte carlo model for crystallization and percolation. *IEEE Transaction on Electronic Device,* **53**(12):3032-3039.

Schroeder, D. (1998). Semiconductor material and Device Characterization, 2nd edition, John Willey and Sons, 217-342 New York.

Schubert, E. F. (1993). Doping in III-V Semi- conductors, Cambridge University Press. Great Britain.

Sharma J., Singh G., Thakur A., Saini G.S.S., Goyal N. and Tripathi S.K. (2005). Preparation and characterization of SnSe nanocrystalline thin Films. *Journal of Optoelectronics and Advanced Materials,* **7**:2085-2094.

Simone, R. Robert, M. Jean,J. Becky, M. Martin, S. Yi-Chou, C. Yen-Hao, S. Erh-Kun, L. Ming-Hsiu, L. (2008). *Microelectronic Engineering*, **81**: 23-30.

Singh A.K., Singh K. and Saxena N.S. (2008). Effect of Annealing on Structures And Effective Thermal Conductivity of $Se_{90}In_{10}$ Chalgogenide Glass. *Journal of Ovonic Research* **4**:107-111.

Smits, M., (1958) Measurement of sheet resistivity with the four point probes, BS Tech. J, 37, P711-718.

Suh D.S., Kim K.H.P., Noh J.S., Shin W.C., Kang Y.S., Kim C., Khang Y. and Yoo I.K. (2006). Critical quenching speed determining phase of $Ge_2Sb_2Te_5$ in phase change memory. *In IEDM Technical Digest,* **30:**2.

Sun Y., Shi J. and Meng Q. (1996). Measurement of sheet resistance of cross micro-areas using a modified Van der Pauw method. *Semiconductor Science and Technology,* **11**(5):805.

Sze, S.M., (1981). Semiconductor Devices, 2nd edition. John Willey & Sons, Inc. USA.

Ting Z., Zhitang S., Feng R., Gaoming F., Bo L.,Songlin F., and BOMY C. High speed Chalcogenide Random Access Memory Based on$Si_2Sb_2Te_5$. *Japanese Journal of applied Physics,* **46**:247-249.

Van der Pauw L.J. (1958). A method of measuring specific resistivity and hall effect of discs of arbitrary shape. *Philips Research Reports,* **13**:1-9.

Van der Pauw L.J. (1958). A method of measuring specific resistivity, and hall coefficient on Lamellae of arbitrary shape. *Philips Technical Review,* **20**:220-224.

Wamwangi D., Njoroge W.K. and Wuttig M. (2002). Crystallization Kinetics of $Ge_4Sb_1Te_5$ films. *Thin Solid Films,* **408**:310-315.

Wang F., Zhang T., Liu C. L., Song Z. T., Wu L. C., Liu B., Feng S. L., and Chen B., (2008). Au doped Sb_3Te phase change material for c-ram device. *Applied Surface Science,* **254**(8):2281-2284.

Wu L.C., Song Z.T., Rao F., Gong Y.F., Liu B., Wang L.Y., Liu W.L. and Feng S.L. (2008). Performance improvement of phase change memory cell with cup-shaped bottom electrode contact. *Applied Physics Letters,* **93**(10):103107.

Wuttig M., Detemple R., Friedrich I., Njoroge W.K., Thomas I., Weidenhof V., Woltgens H.W. and Ziegler S. (2002). The quest for fast phase change materials. *Journal of Magnetism and Magnetic Materials,* **249**:492-498.

Yamada N., Ohno E., K., Akahira., Nishiuchi K., Nagata K. and Takao M. (1987). High speed overwritable phase change optical disk material. *Japanese Journal of Applied Physics,* **26**(4):61-66.

Yamada N., Ohno E., Nishiuchi K., Akahira N. and Takao M. (1991). Rapid phase transitions of GeTe-Sb_2Te_3 Pseudobinary amorphous thin films for an optical disc memory. *Journal of Applied Physics,* **69**(5):2849-2856.

Yu, P. Y., Cardona, M. (1996). Fundamentals of semi conductors. Springer-Verlag, Berlin Heidelberg. 233-280.

APPENDICES

Appendix 1: Edwards AUTO 306 Vacuum coater

Appendix 2: Photograph of Alpha IQ Surface Profiler

Appendix 3: Photograph of the set used during thermal annealing